NACA RM L9K08

NACA

RESEARCH MEMORANDUM

STABILITY AND CONTROL CHARACTERISTICS AT LOW SPEED OF A $\frac{1}{4}$-SCALE BELL X-5 AIRPLANE MODEL

LONGITUDINAL STABILITY AND CONTROL

By William B. Kemp, Jr., Robert E. Becht, and
Albert G. Few, Jr.

Langley Aeronautical Laboratory
Langley Air Force Base, Va.

NATIONAL ADVISORY COMMITTEE
FOR AERONAUTICS

WASHINGTON

March 14, 1950

NACA RM L9K08

NATIONAL ADVISORY COMMITTEE FOR AERONAUTICS

RESEARCH MEMORANDUM

STABILITY AND CONTROL CHARACTERISTICS AT LOW SPEED OF A $\frac{1}{4}$-SCALE BELL X-5 AIRPLANE MODEL

LONGITUDINAL STABILITY AND CONTROL

By William B. Kemp, Jr., Robert E. Becht, and
Albert G. Few, Jr.

SUMMARY

An investigation was made of the low-speed longitudinal stability and control characteristics of a $\frac{1}{4}$-scale model of a preliminary Bell X-5 airplane design with various leading-edge slat and trailing-edge flap arrangements. The model exhibited a marked increase in stability with increasing sweep angle at low lift coefficients. The trimmed maximum lift coefficient without slats or flaps increased with increasing sweep angle. The increases in trimmed maximum lift coefficient produced by the slats or flaps decreased rapidly with increasing sweep angle and became approximately zero at 60° sweep. At large sweep angles, the rate of increase of drag coefficient with lift coefficient was considerably greater than that predicted by the lifting-line induced-drag equation.

INTRODUCTION

An investigation of the stability and control characteristics at low speed of a $\frac{1}{4}$-scale model of a preliminary Bell X-5 airplane design has been conducted in the Langley 300 MPH 7- by 10-foot tunnel. The X-5 airplane is a proposed research airplane incorporating wings for which sweepback angle can be varied continuously between 20° and 60°. Provision for longitudinal translation of the wing with respect to the fuselage is also made.

The present paper contains the results of the longitudinal stability and control tests of the model at four sweep angles and with various leading-edge slat and trailing-edge flap arrangements. A limited analysis of the results is presented in the present paper.

SYMBOLS

The system of axes employed, together with an indication of the positive forces, moments, and angles, is presented in figure 1. The symbols used in this paper are defined as follows:

C_L	lift coefficient (Lift/qS)
C_X	longitudinal force coefficient (X/qS)
$C_{D_o} = -C_X$ at $C_L = 0$	
C_m	pitching-moment coefficient ($M/qS\bar{c}_{50}$)
X	longitudinal force along X-axis, pounds
Y	lateral force along Y-axis, pounds
Z	force along Z-axis (lift equals -Z), pounds
L	rolling moment about X-axis, foot-pounds
M	pitching moment about Y-axis, foot-pounds
N	yawing moment about Z-axis, foot-pounds
q	free-stream dynamic pressure, pounds per square foot ($\rho V^2/2$)
S	wing area, square feet
$\bar{c}$	wing mean aerodynamic chord based on wing plan form shown in figure 2, feet
$\bar{c}_{50}$	wing mean aerodynamic chord at 50° sweep, feet
b	wing span, feet
V	free-stream velocity, feet per second

A	aspect ratio (b^2/S)
ρ	mass density of air, slugs per cubic foot
α	angle of attack of thrust line, degrees
i_t	angle of incidence of stabilizer with respect to thrust line, degrees
δ	control-surface deflection measured in a plane perpendicular to hinge line, degrees
Λ	angle of sweepback of quarter-chord line of unswept wing panel, degrees

Subscripts:

e	elevator
r	rudder
a	aileron
f	flap

APPARATUS AND METHODS

Description of Model

The model used in the present investigation was a $\frac{1}{4}$-scale model of a preliminary Bell X-5 design and must, therefore, be considered only qualitatively representative of the Bell X-5 airplane.

Physical characteristics of the model are presented in figure 2, and photographs of the model on the support strut are given in figure 3. Figure 4 includes details of the various slats and flaps investigated. The model was constructed of wood bonded to steel reinforcing members.

The wing panels were pivoted about an axis normal to the wing-panel chord plane. Thus, the wing incidence measured in a streamwise direction was zero for all sweep angles. At all sweep angles, the wing was located so that the quarter chord of the mean aerodynamic chord fell at a fixed fuselage station. The moment reference center was located at this same fuselage station. (See fig. 2.)

The jet-engine ducting was simulated on the model by the use of an open, straight tube having an inside diameter equal to that of the jet exit and extending from the nose to the jet exit.

Tests

The tests were conducted in the Langley 300 MPH 7- by 10-foot tunnel at a dynamic pressure of 34.15 pounds per square foot which corresponds to a Mach number of 0.152 and a Reynolds number of 2,000,000 based on the mean aerodynamic chord of the wing at 50° sweep for average test conditions.

During the tests, no control was imposed on the flow quantity through the jet duct. It is probable, therefore, that the inlet velocity ratio had values somewhat less than 1.0.

Corrections

The angle-of-attack, drag, and pitching-moment results have been corrected for jet-boundary effects computed on the basis of unswept wings by the methods of reference 1. Independent calculations have shown that the effects of sweep on the above corrections are negligible. All coefficients have been corrected for blocking by the model and its wake by the method of reference 2.

Corrections for the tare forces and moments produced by the support strut have not been applied. It is probable, however, that the significant tare corrections would be limited to small increments in pitching moment and drag.

Vertical buoyancy on the support strut, tunnel air-flow misalinement, and longitudinal-pressure gradient have been accounted for in computation of the test data.

RESULTS AND DISCUSSION

The aerodynamic coefficients presented herein are based on the wing area of the sweep configuration in question and on the mean aerodynamic chord of the wing at 50° sweep. Thus, the lift and longitudinal-force coefficients are of the usual form; whereas the pitching-moment coefficients are based on a reference length which is fixed in the fuselage and is independent of the wing sweep angle.

Basic Longitudinal Characteristics

Results of the pitch tests of the model in the clean configuration at four sweep angles are presented in figure 5. At 20° sweep, the lift and pitching-moment characteristics were essentially linear below the stall, especially with the horizontal tail removed. As the sweep angle was increased (and the aspect ratio reduced) the nonlinearities in the lift and pitching-moment characteristics usually associated with high sweep and low aspect ratio were observed. At all sweep angles greater than 20°, the relationship between sweep angle and aspect ratio was such that a tendency toward longitudinal instability at high lift coefficients would be anticipated from the considerations of reference 3. This trend was apparent at lift coefficients above 0.6. As the wing stalled, however, the tail contributed a strong stabilizing moment at all sweep angles, apparently caused by a loss of downwash at the tail.

At lift coefficients near zero, the model exhibited a marked increase in stability with increasing sweep. The aerodynamic center of the wing-fuselage combination moved from $0.22\bar{c}_{50}$ or $0.20\bar{c}$ at 20° sweep to $0.36\bar{c}_{50}$ or $0.34\bar{c}$ at 60° sweep. The theoretical calculations of reference 4 indicate an aerodynamic-center movement of less than $0.02\bar{c}$ for the wings alone. Thus, a strong wing-fuselage interference effect is indicated.

The tail-off maximum lift coefficient increased with increasing sweep angle, varying from 0.85 at 20° sweep to 1.11 at 60° sweep. The trimmed maximum lift coefficient can be approximated by extrapolating the $C_{L_{max}}$ values for the various stabilizer settings to zero pitching moment assuming that a sufficient range of stabilizer angle is available. The values of trimmed $C_{L_{max}}$ thus obtained varied from 0.86 at 20° sweep to 1.01 at 60° sweep.

The longitudinal-force results of figure 5 indicate that the minimum drag coefficient of the model was relatively independent of sweep angle. The drag rise with lift coefficient, however, was considerably greater at the high sweep angles than the induced drag calculated by the usual lifting-line equation for zero sweep and indicated by the dashed curves. Thus, the profile drag at high sweep angles increased appreciably with lift coefficient even at low lift coefficients.

Characteristics of the model with the wings removed are presented in figure 6. The coefficients were computed using the wing area at 60° sweep. For comparison with data at other sweep angles, the coefficient values should be multiplied by the ratio of wing areas.

Leading-Edge Slats

Figures 7 to 10 illustrate the effect of the leading-edge slat configurations tested at each sweep angle. Slat position A was selected from slat data on unswept wings to give the optimum increment in $C_{L_{max}}$. Slat position B represents a compromise configuration intended to simplify the structural problem of slat installation. Details of the two slat configurations are shown in figure 4.

At 20° sweep, slat A produced an increment in useful $C_{L_{max}}$ of about 0.50 while slat B caused an increment of about 0.32. The increments in $C_{L_{max}}$ produced by the slats were essentially unchanged by flap deflection. As the sweep angle was increased, the effectiveness of the slats in increasing $C_{L_{max}}$ decreased rapidly, showing essentially no effectiveness at 60° sweep. It is of interest to note, however, that at large sweep angles slats could produce a drag reduction at moderate and high lift coefficients indicating their possible use for drag reduction in accelerated maneuvers.

At all sweep angles, the slats produced a small decrease in longitudinal stability over most of the lift-coefficient range. At 60° sweep the slats served to decrease the variation of longitudinal stability with lift coefficient.

Figures 11 and 12 present the results of stabilizer tests at 20° and 60° sweep with slat A. The tests of figure 12(b) were made with only the outboard half of the slat extended to position A. The outboard slat was effective in eliminating the trend toward instability at high lift coefficients but it also increased the pitching-moment coefficient required from the tail to trim at high lift coefficients.

Trailing-Edge Flaps

The characteristics of the three different flap configurations shown in figure 4 were determined at 20° sweep. Flap A was a slotted flap whereas flaps B and C were split flaps. Flap B was so located that its inboard end was coincident with the wing-fuselage intersection at 60° sweep. Flap C was identical with flap B except that the inboard end was extended to intersect the fuselage at 20° sweep.

The longitudinal characteristics at 20° sweep presented in figure 13 for various deflections of flap B indicate that only small changes in $C_{L_{max}}$ were produced by varying the flap deflection between 40° and 60°. A deflection of 50° was chosen for the remainder of the flap tests.

The longitudinal characteristics at 20° sweep with the three flap configurations are given in figure 14 for the slats extended to position A. Flaps A and B were about equally effective in increasing the trimmed $C_{L_{max}}$; whereas flap C with its greater area, produced a correspondingly larger increment in $C_{L_{max}}$. Comparison with the data of figure 11 indicates that each flap produced a small increase in stability at moderate lift coefficients with flaps A and B remaining stable through the stall. With flap C, however, some instability at the stall is evident. With the horizontal tail off, each flap produced a nose-down increment in pitching-moment coefficient, the smallest increment being produced by flap B. When the horizontal tail was added, flap B still showed a smaller nose-down trim change than flap A, but the large downwash behind flap C resulted in a nose-up trim change. The flap characteristics at 20° sweep with the slats retracted are presented in figure 15.

The characteristics of the model at 50° and 60° sweep with flap B are presented in figures 16 and 17, respectively. Comparison with figures 5(c) and 5(d) indicates that the increase in trimmed $C_{L_{max}}$ caused by flap deflection was very small at 50° sweep and was essentially zero at 60° sweep. At lift coefficients less than the maximum, flap deflection reduced the angle of attack required for a given lift coefficient but comparison of the drag results shows that this reduction in angle of attack was not enough to produce any appreciable drag reduction.

Longitudinal Control

The effect of elevator deflection on the characteristics of the model at 20° and 60° sweep is shown in figure 18. At both sweep angles the variation of pitching-moment coefficient with elevator deflection was smooth although not quite linear. At 20° sweep, the elevator power was sufficient for trim over the lift-coefficient range obtained even for a center-of-gravity location considerably removed from that used in the tests. At 60° sweep, the stability of the model was such that the elevator power was not quite adequate to trim at $C_{L_{max}}$ with the stabilizer incidence used.

Comparison of figures 5 and 18 shows some small discrepancies between the two sets of data at zero elevator deflection, the discrepancies occurring mainly at high lift coefficients. The trimmed maximum lift coefficients measured for 20° sweep from figures 5 and 18 differ by about 0.06. This difference may be contributed to, in a small degree, by the change in tail center-of-pressure location when using the elevator rather than the stabilizer as a trim device. The major contribution to the discrepancies noted, however, is believed to arise from small inaccuracies in setting the slat in its retracted position, thus producing changes in the wing leading-edge contour.

CONCLUSIONS

An investigation at low speed of the longitudinal stability and control of a $\frac{1}{4}$-scale model of a preliminary X-5 airplane design indicates the following conclusions:

1. The aerodynamic center of the wing-fuselage combination at low lift coefficients moved from $0.20\bar{c}$ at 20° sweep to $0.34\bar{c}$ at 60° sweep. This movement is considerably greater than that predicted by potential theory indicating the possibility of a strong wing-fuselage interference effect.

2. The trimmed maximum lift coefficient without slats or flaps increased with increasing sweep angle.

3. At large sweep angles, the rate of increase of drag coefficient with lift coefficient was considerably greater than that predicted by the lifting-line induced-drag equation.

4. The increases in trimmed maximum lift coefficient produced by leading-edge slats or trailing-edge flaps decreased rapidly with increasing sweep angle and became approximately zero at 60° sweep.

Langley Aeronautical Laboratory
National Advisory Committee for Aeronautics
Langley Air Force Base, Va.

REFERENCES

1. Gillis, Clarence L., Polhamus, Edward C., and Gray, Joseph L., Jr.: Charts for Determining Jet-Boundary Corrections for Complete Models in 7- by 10-Foot Closed Rectangular Wind Tunnels. NACA ARR L5G31, 1945.

2. Herriot, John G.: Blockage Corrections for Three-Dimensional-Flow Closed-Throat Wind Tunnels, with Consideration of the Effect of Compressibility. NACA RM A7B28, 1947.

3. Soulé, Hartley A.: Influence of Large Amounts of Wing Sweep on Stability and Control Problems of Aircraft. NACA TN 1088, 1946.

4. DeYoung, John: Theoretical Additional Span Loading Characteristics of Wings with Arbitrary Sweep, Aspect Ratio, and Taper Ratio. NACA TN 1491, 1947.

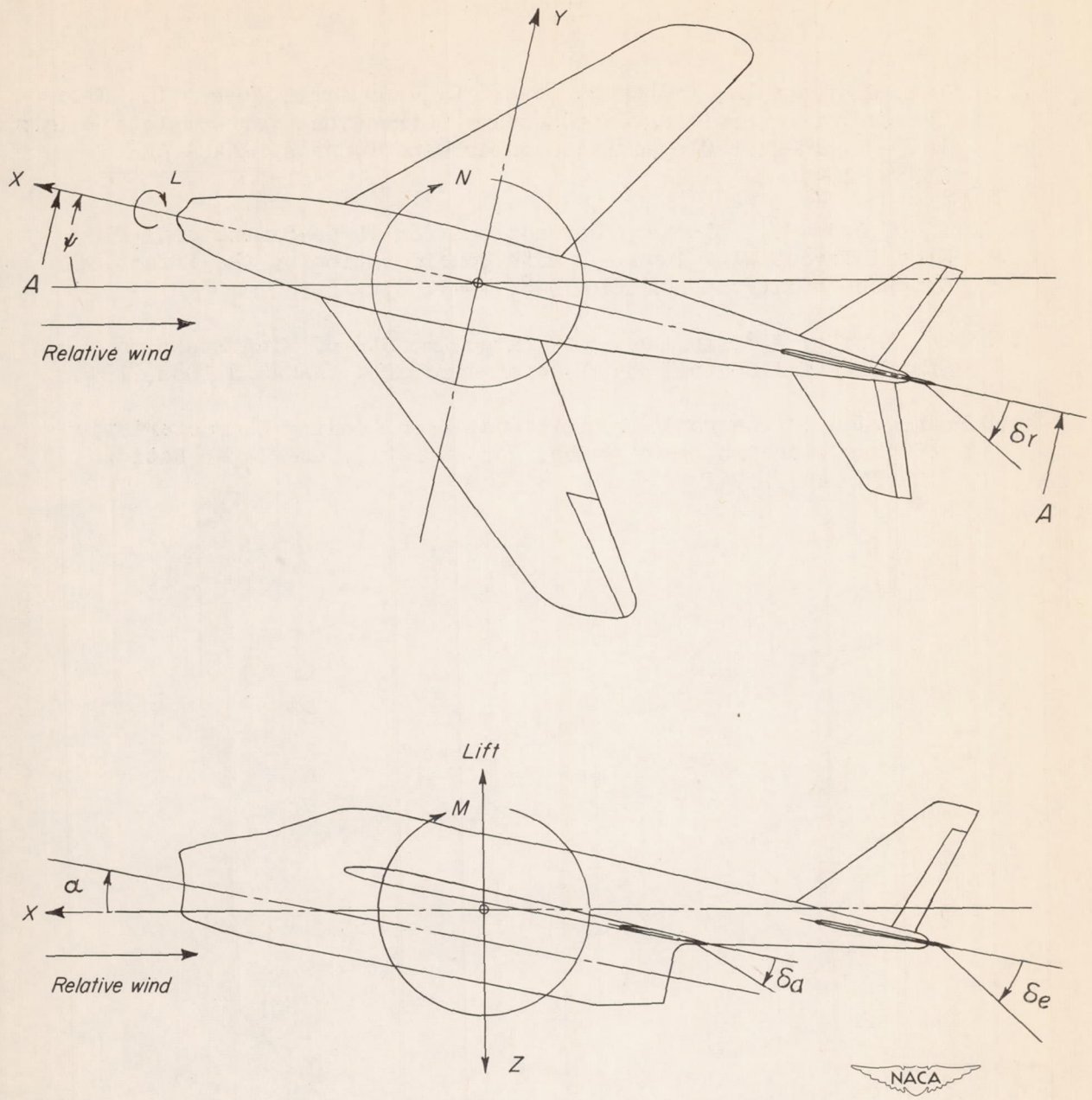

Figure 1.- System of axes and control-surface deflections. Positive values of forces, moments, and angles are indicated by arrows.

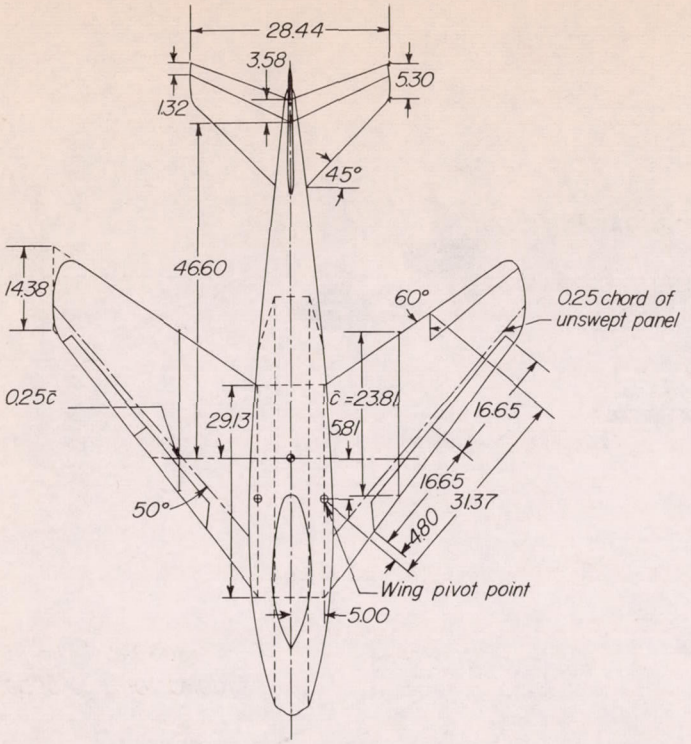

Physical characteristics

Wing

Sweep, deg	20	35	50	60
Area, sq ft	10.33	10.45	10.80	11.33
Aspect ratio	5.76	4.56	2.98	1.92
Span, ft	7.72	6.90	5.67	4.66
Mean aerodynamic chord, ft	1.396	1.579	1.985	2.535

Incidence, deg	0
Dihedral, deg	-2
Airfoil section perpendicular to 0.25c	
Root	NACA 64-0103
Tip	NACA 64-008

Horizontal tail

Area, sq ft	1.94
Aspect ratio	2.89

Vertical tail

Area, sq ft	1.33
Aspect ratio	1.46

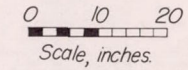

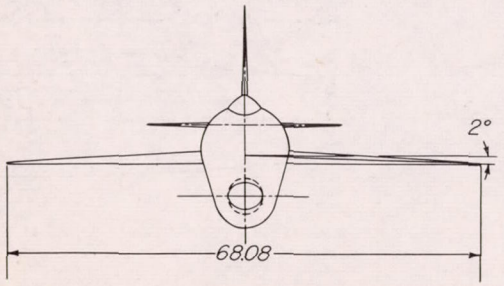

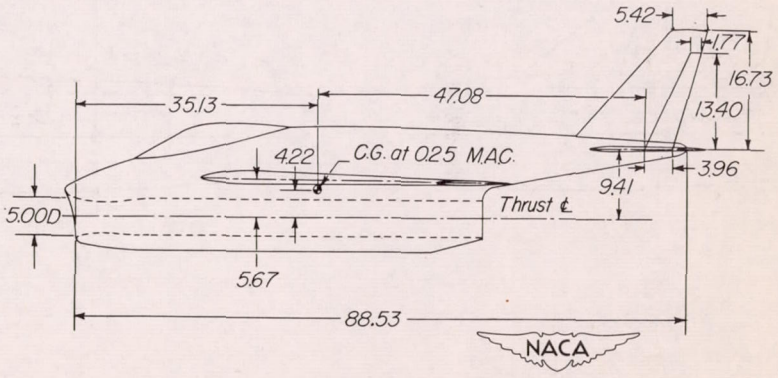

Figure 2.- General arrangement of test model.

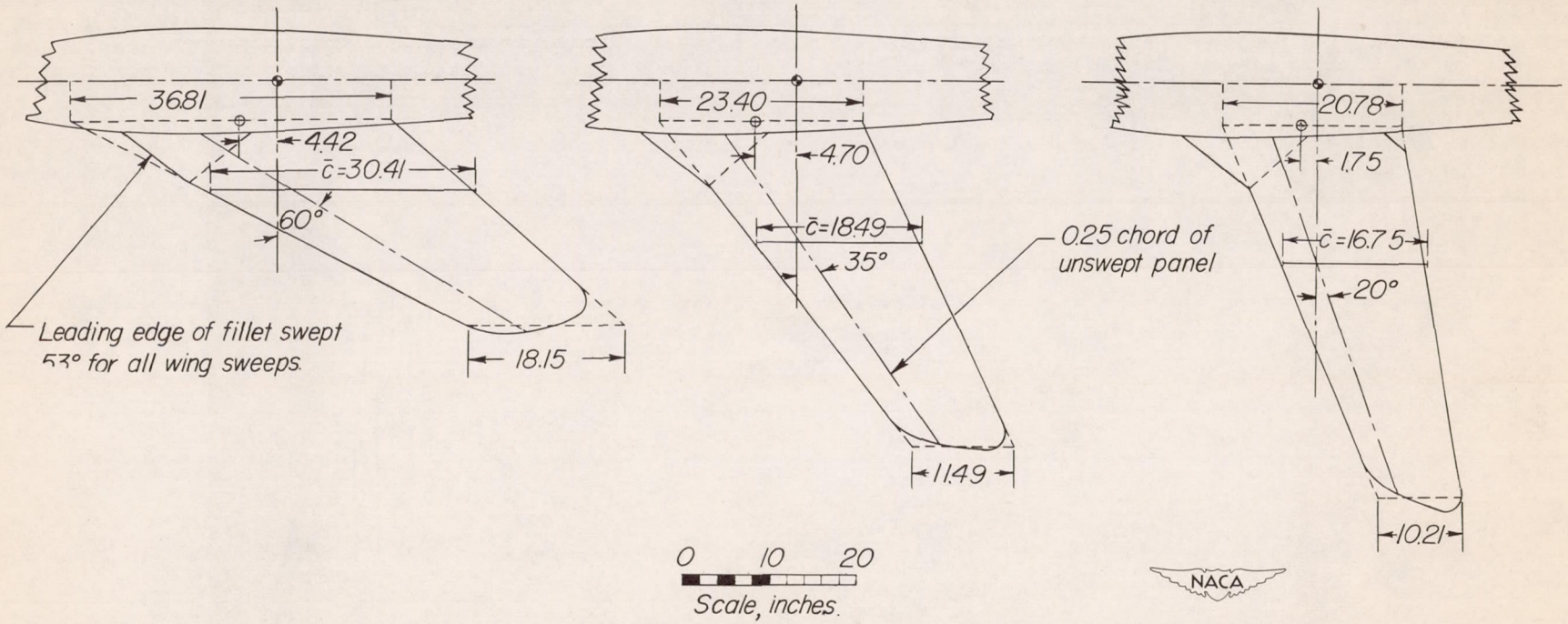

Figure 2.- Concluded.

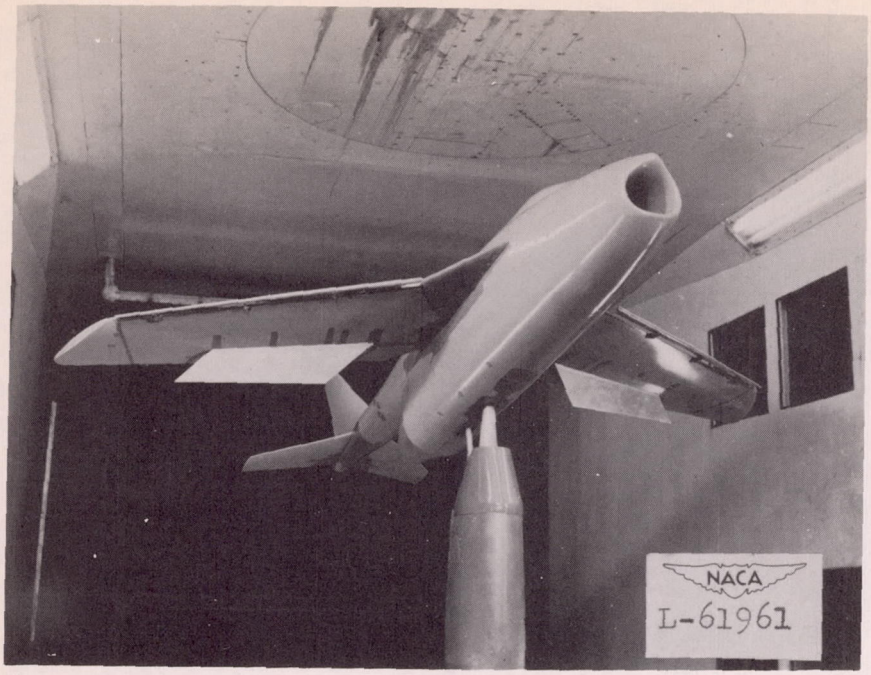

(a) Slat extended; flap B; $\Lambda = 20^{\circ}$.

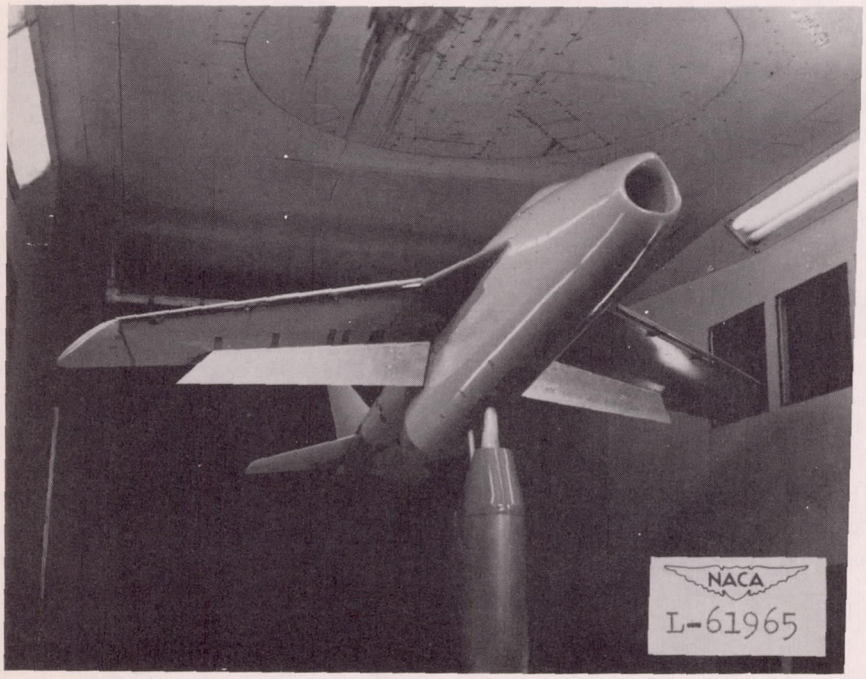

(b) Slat extended; flap C; $\Lambda = 20^{\circ}$.

Figure 3.- Views of test model mounted in tunnel.

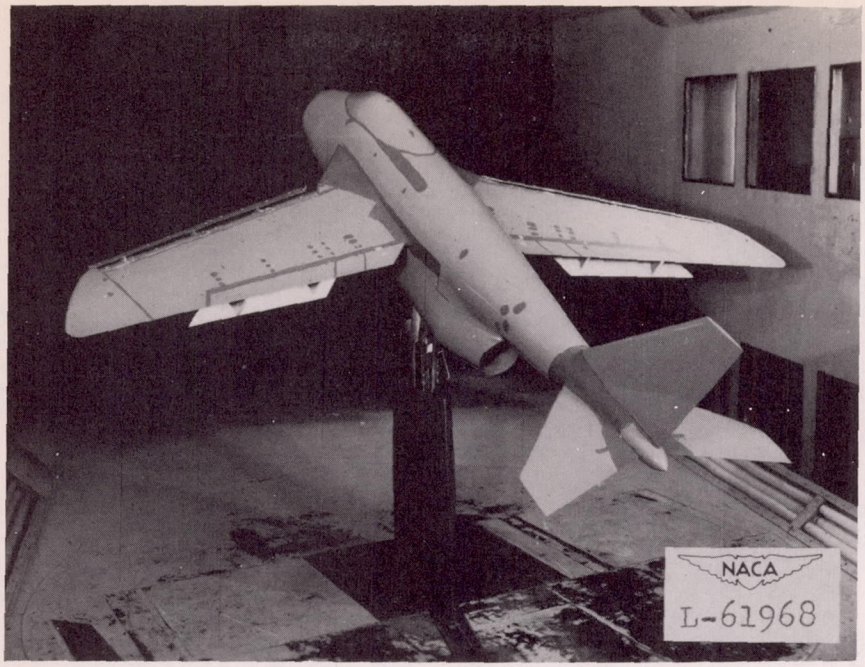

(c) Slat extended; flap B; $\Lambda = 20^{\circ}$.

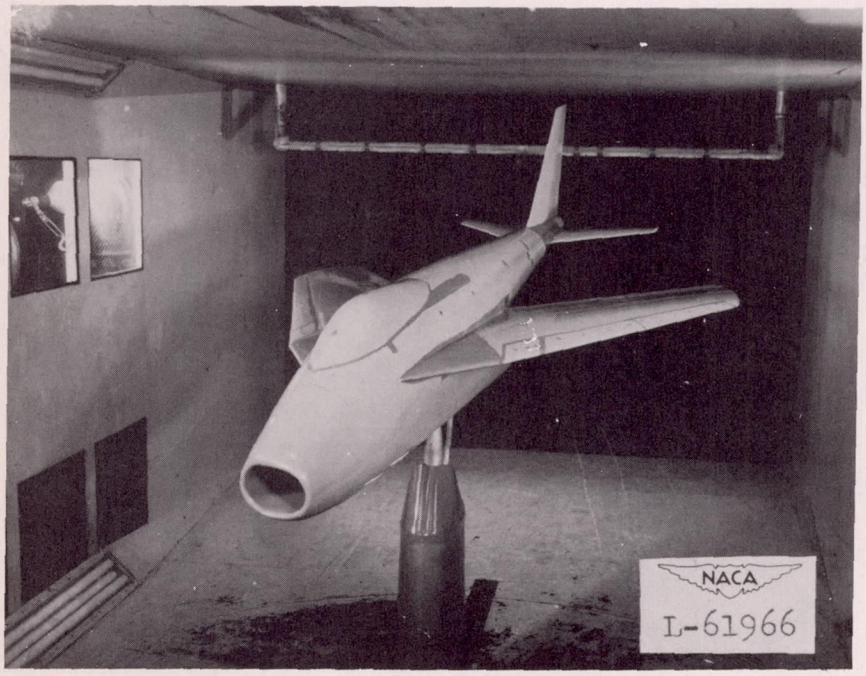

(d) Slats retracted; $\delta_f = 0$; $\Lambda = 60^{\circ}$.

Figure 3.- Concluded.

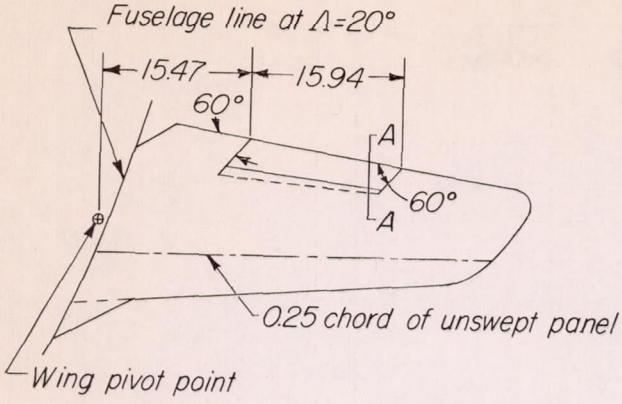

Flap A (slotted)

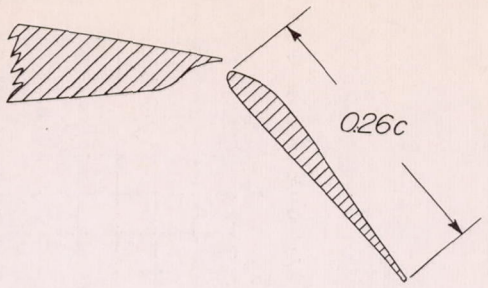

Section A-A

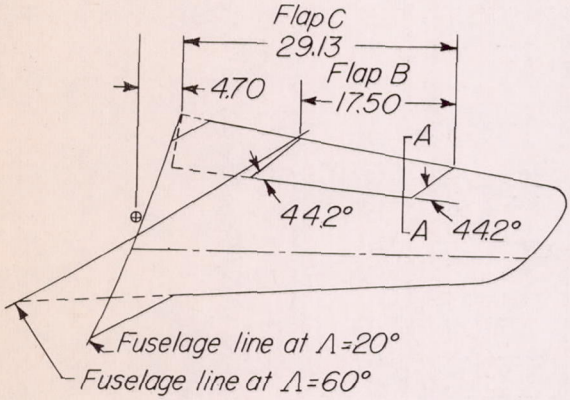

Flap B and C (split)

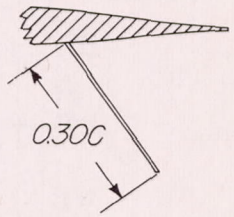

Section A-A

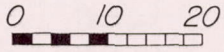

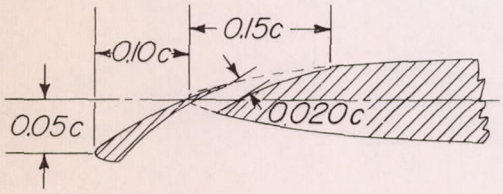

Slat A

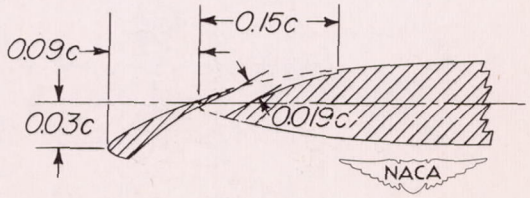

Slat B

Figure 4.- Details of flaps and slats.

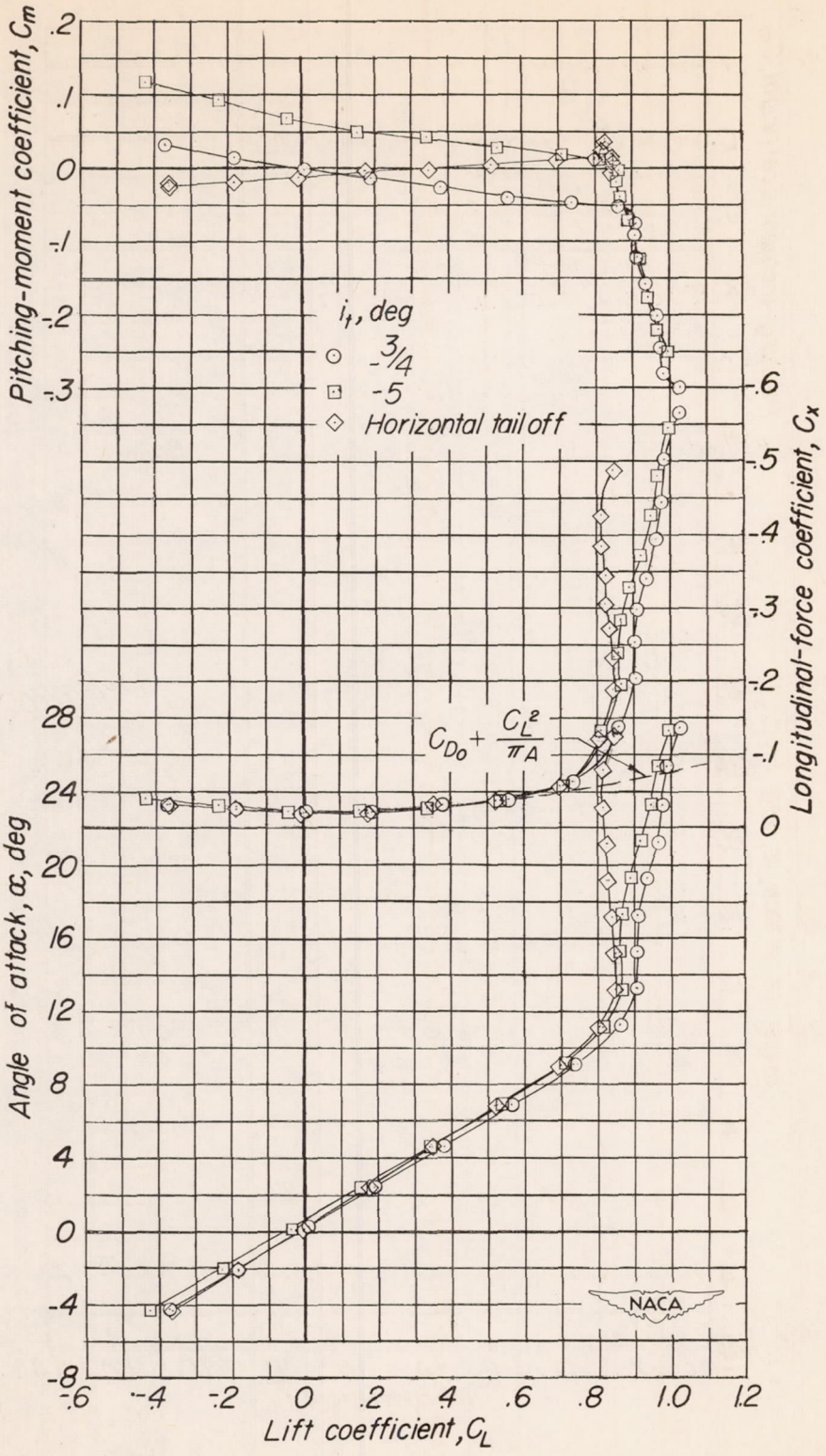

(a) $\Lambda = 20^\circ$.

Figure 5.- The effect of tail incidence on the aerodynamic characteristics of the test model. Slats retracted; $\delta_f = 0$.

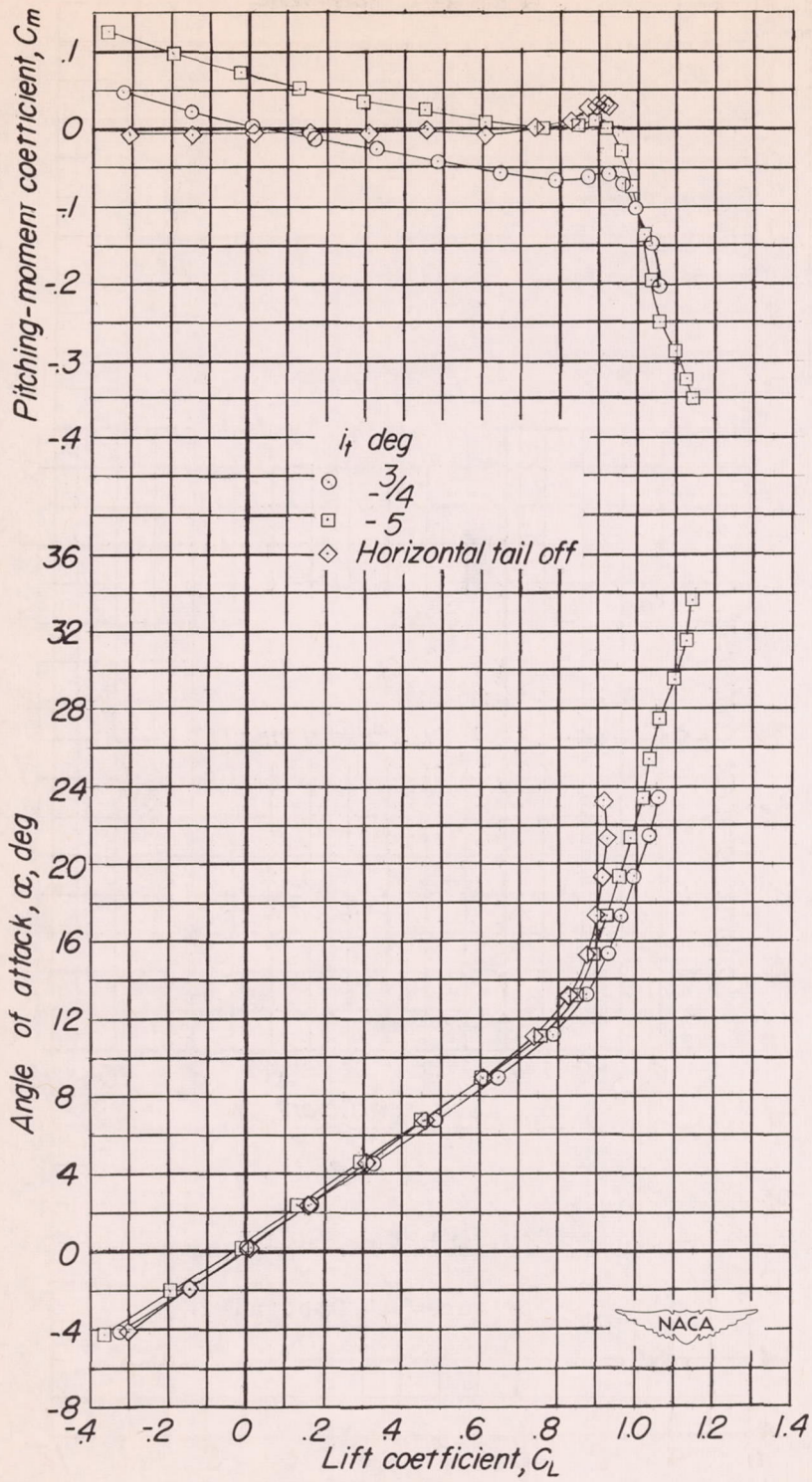

(b) $\Lambda = 35^\circ$.

Figure 5.- Continued.

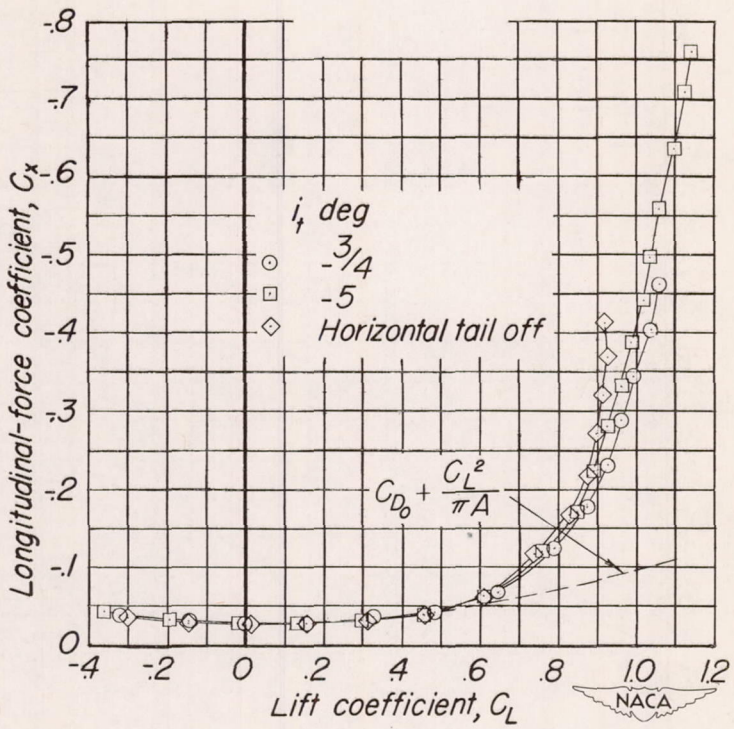

(b) Concluded.

Figure 5.- Continued.

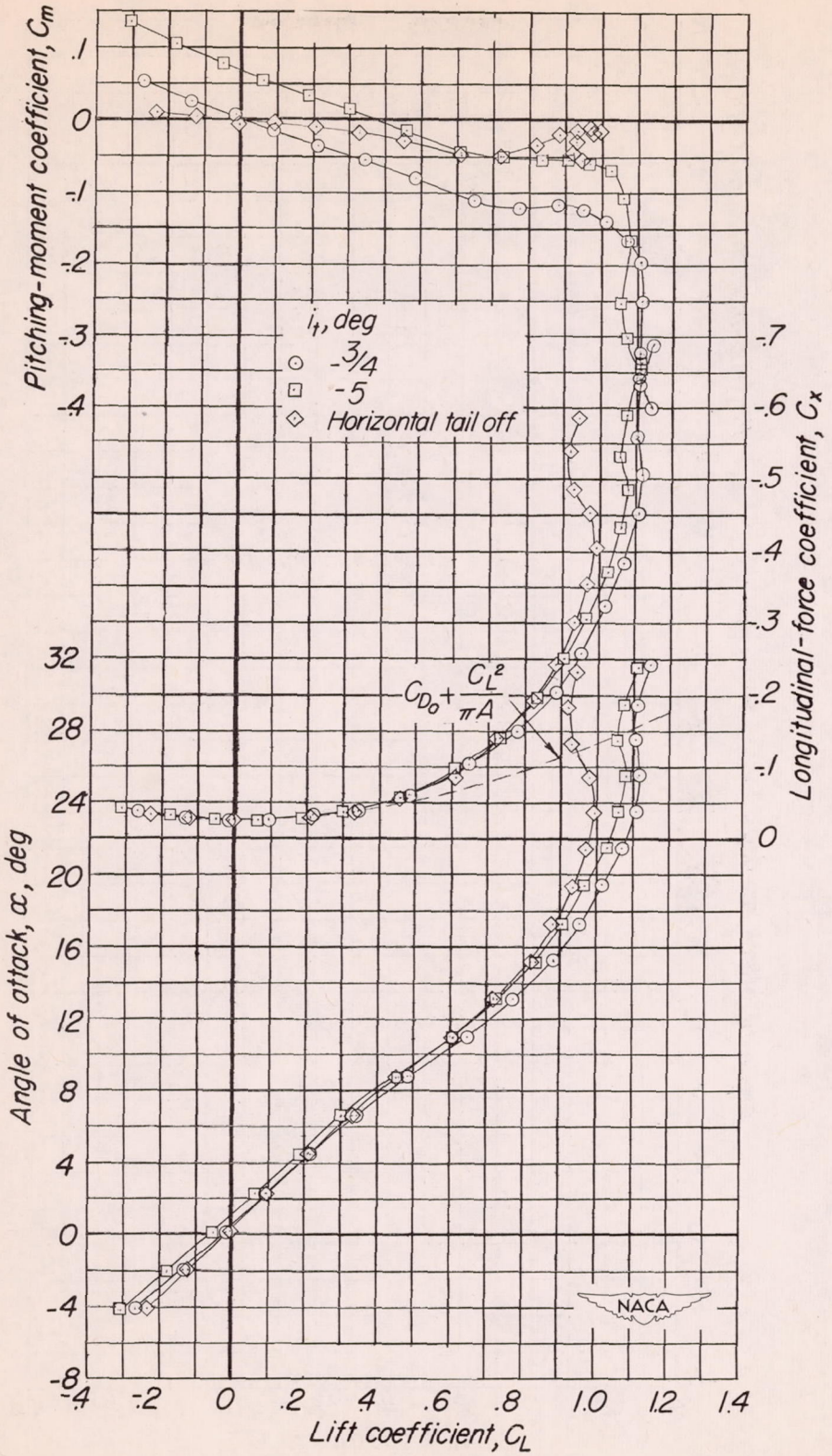

(c) $\Lambda = 50^\circ$.

Figure 5.- Continued.

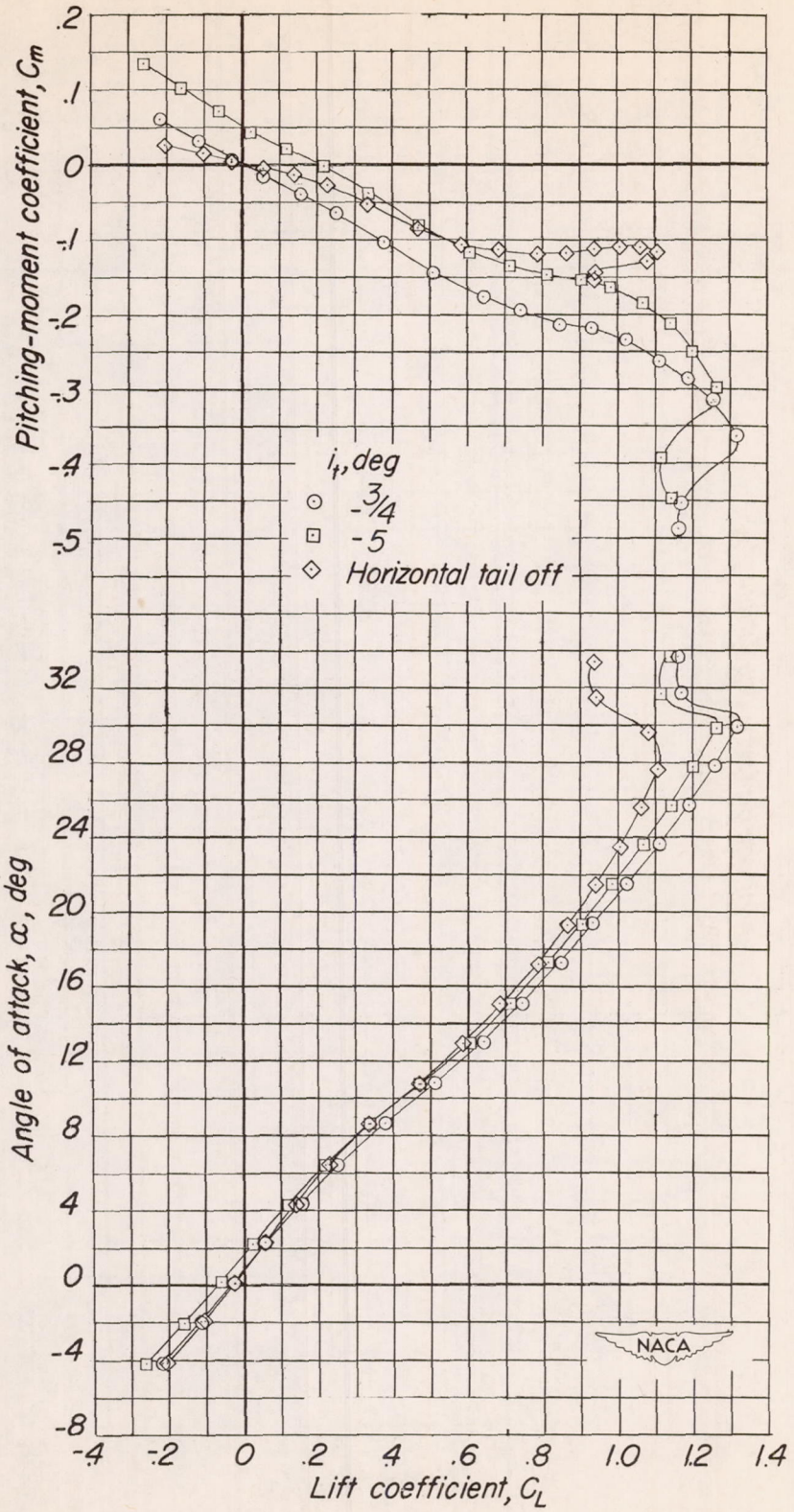

(d) $\Lambda = 60^\circ$.

Figure 5.- Continued.

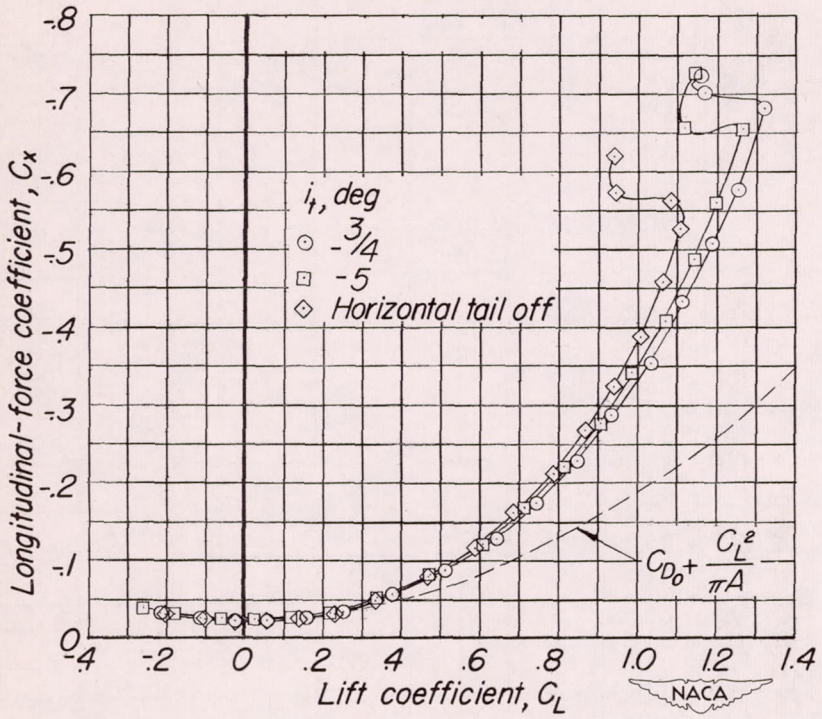

(d) Concluded.

Figure 5.- Concluded.

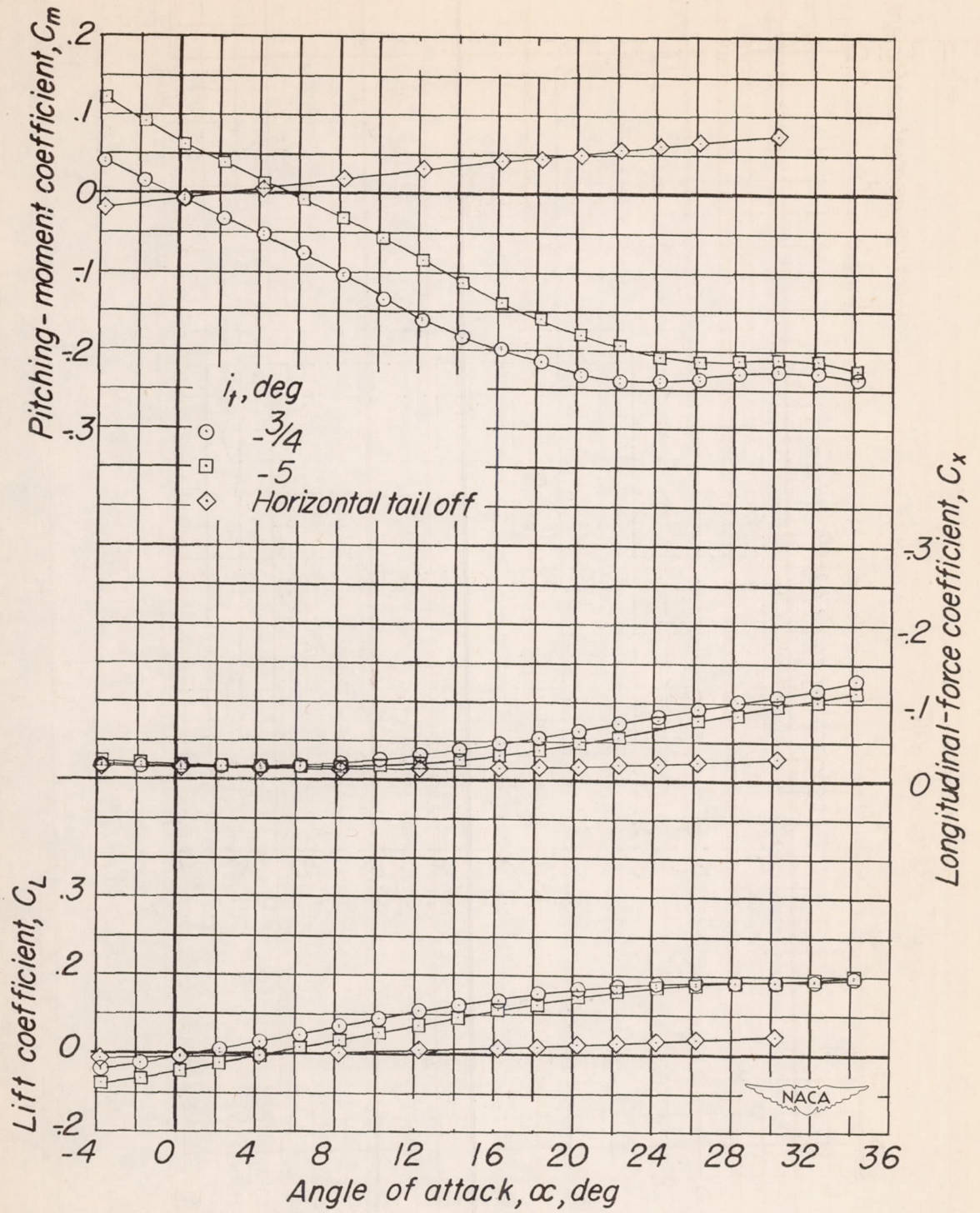

Figure 6.- The effect of tail incidence on the aerodynamic characteristics of the test model with wings removed.

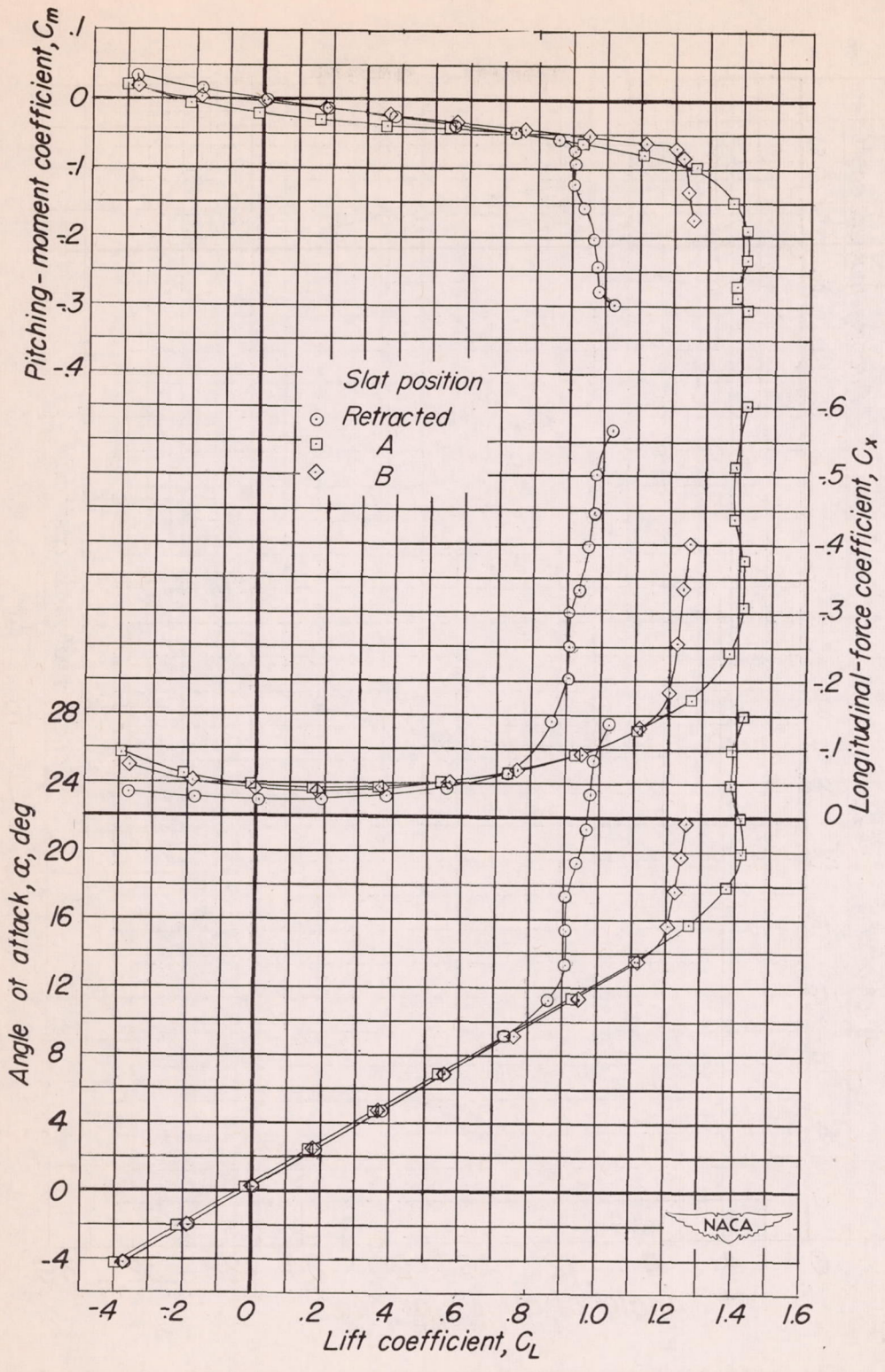

(a) $\delta_f = 0$.

Figure 7.- The effect of slat position on the aerodynamic characteristics of the test model. $\Lambda = 20^\circ$; $i_t = -\frac{3}{4}^\circ$.

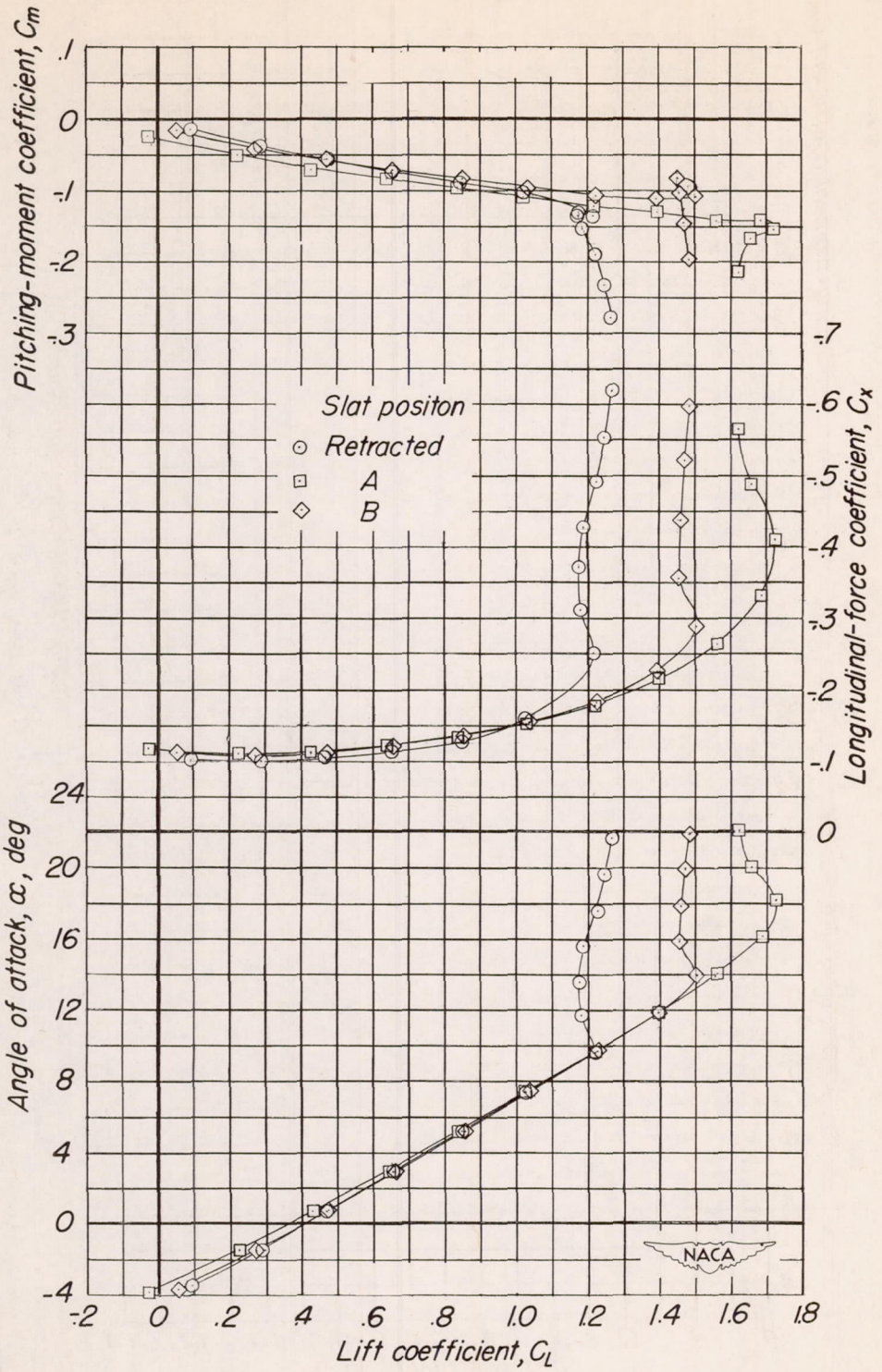

(b) δ_f = 50; flap B.

Figure 7.- Concluded.

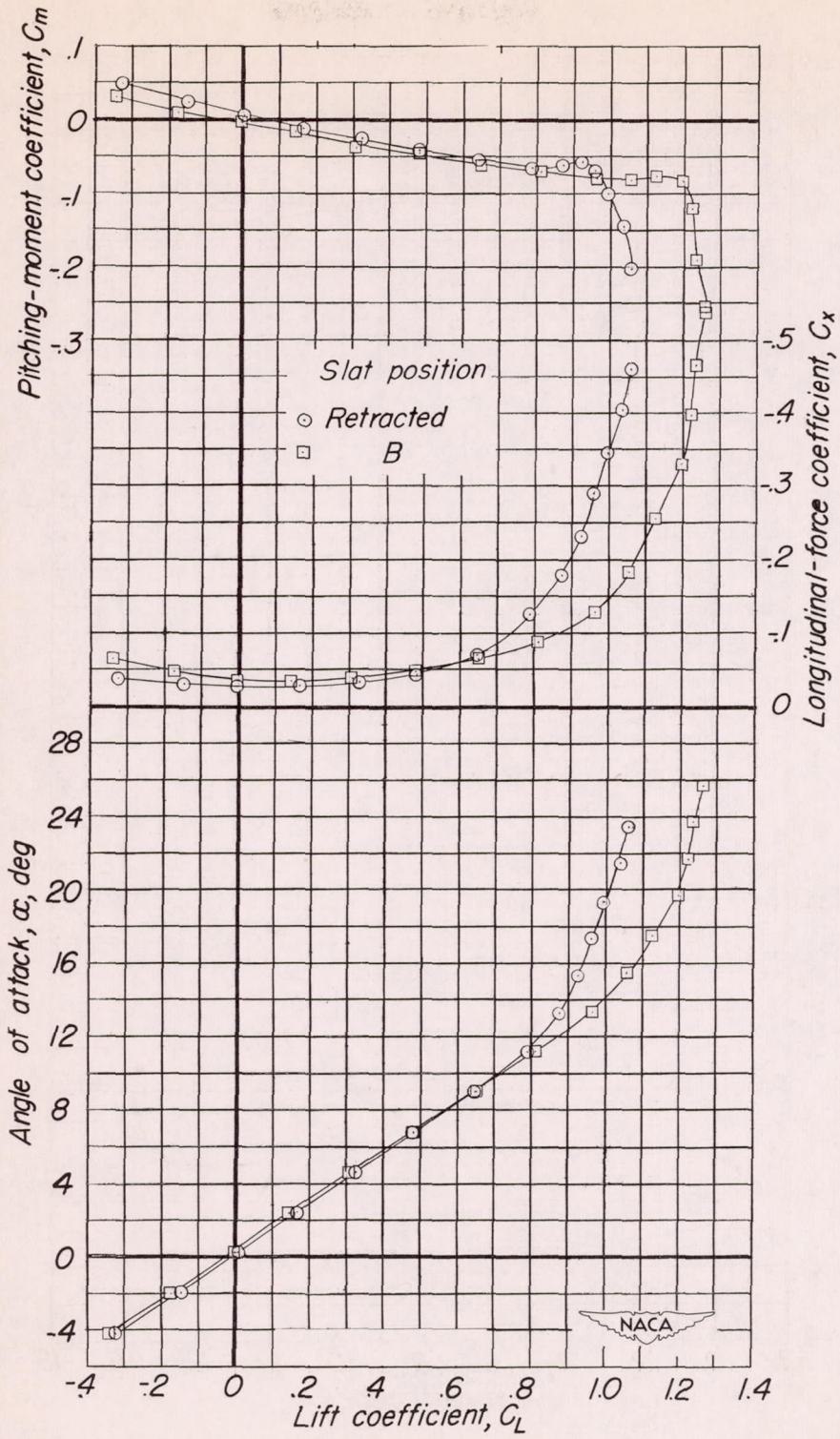

(a) $\delta_f = 0$.

Figure 8.- The effect of slat position on the aerodynamic characteristics of the test model. $\Lambda = 35^\circ$; $i_t = -\frac{3}{4}^\circ$.

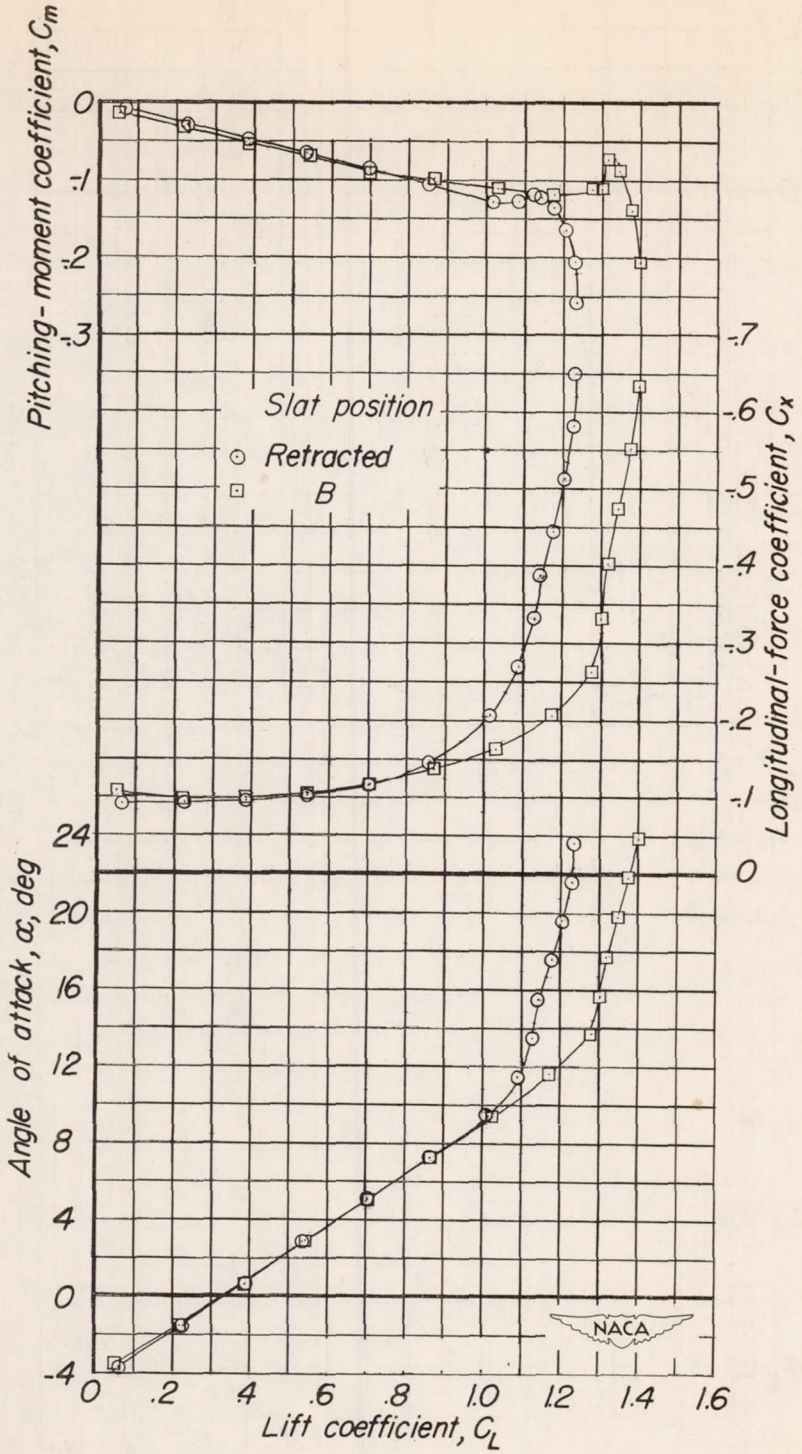

(b) δ_f = 50; flap B.

Figure 8.- Concluded.

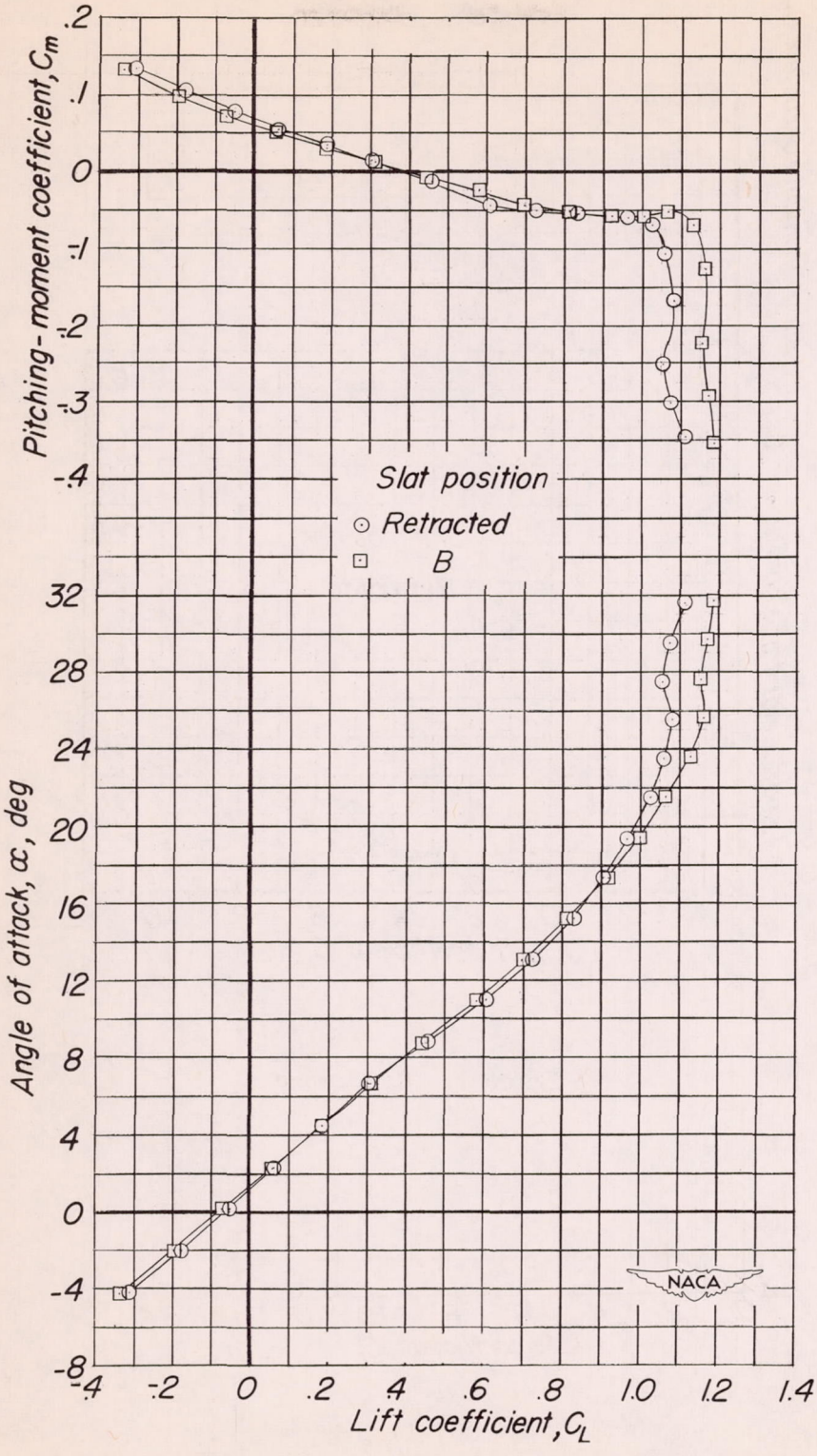

Figure 9.- The effect of slat position on the aerodynamic characteristics of the test model. $\Lambda = 50^\circ$; $i_t = -\frac{3}{4}^\circ$; $\delta_f = 0$.

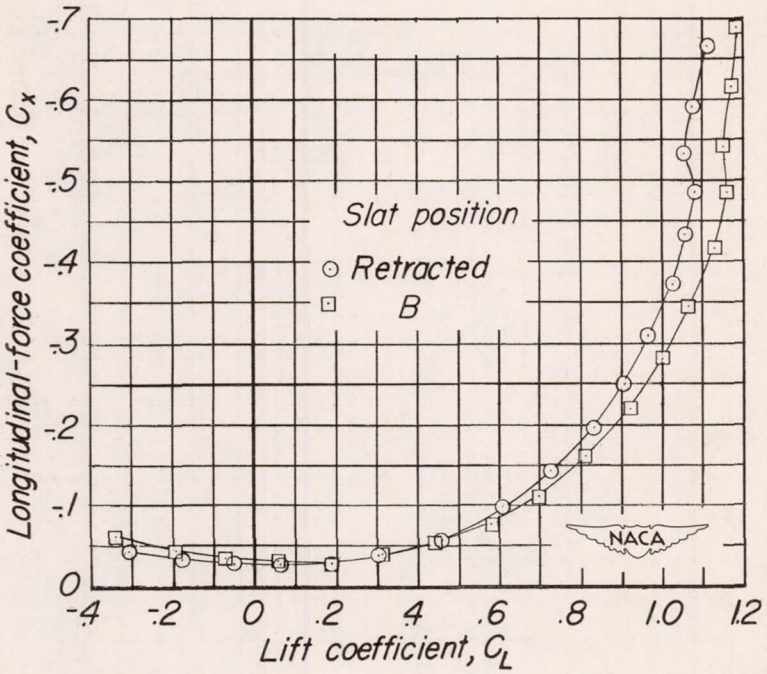

Figure 9.- Concluded.

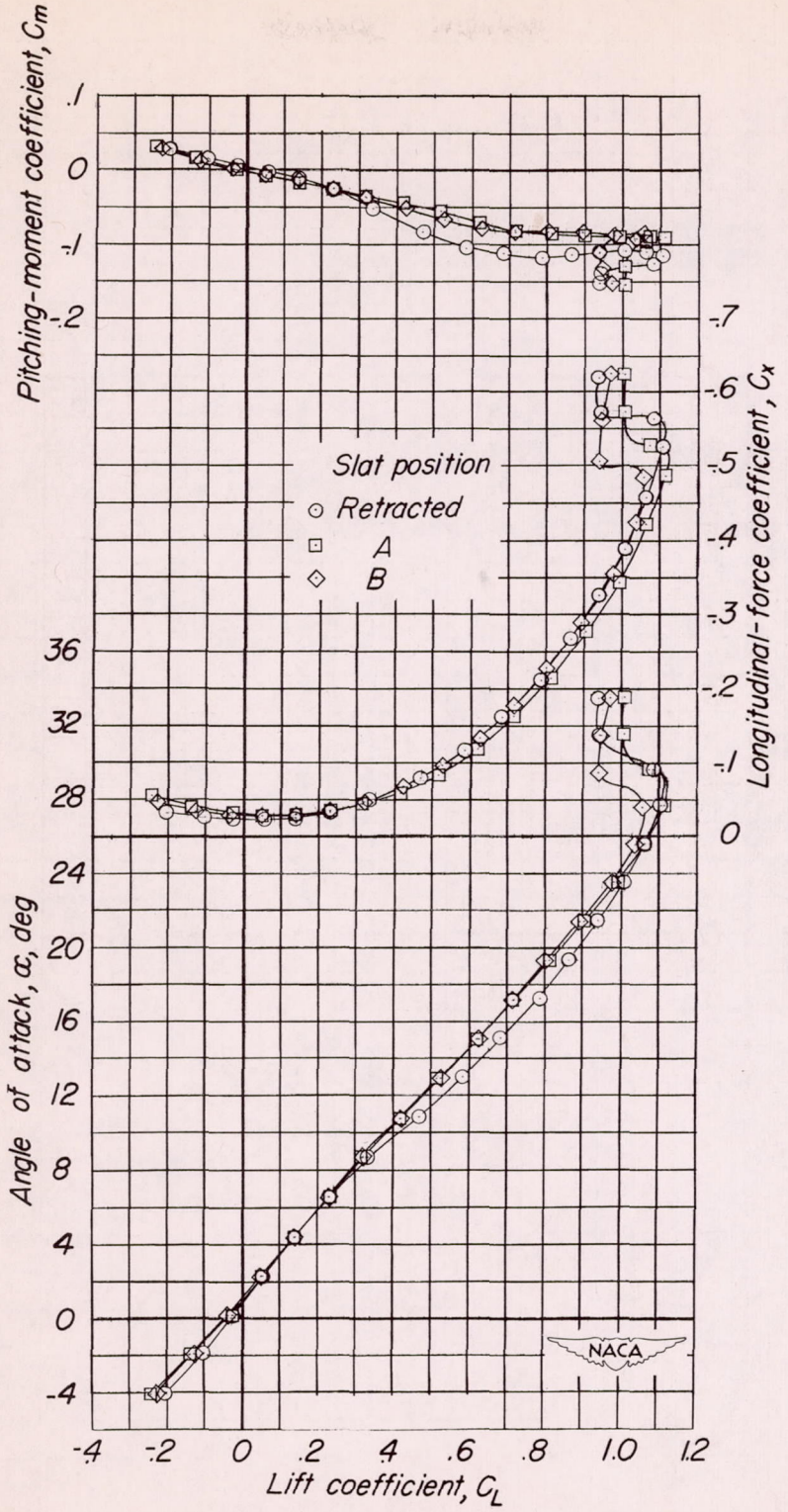

Figure 10.- The effect of slat position on the aerodynamic characteristics of the test model. $\Lambda = 60^\circ$; horizontal tail off; $\delta_f = 0$.

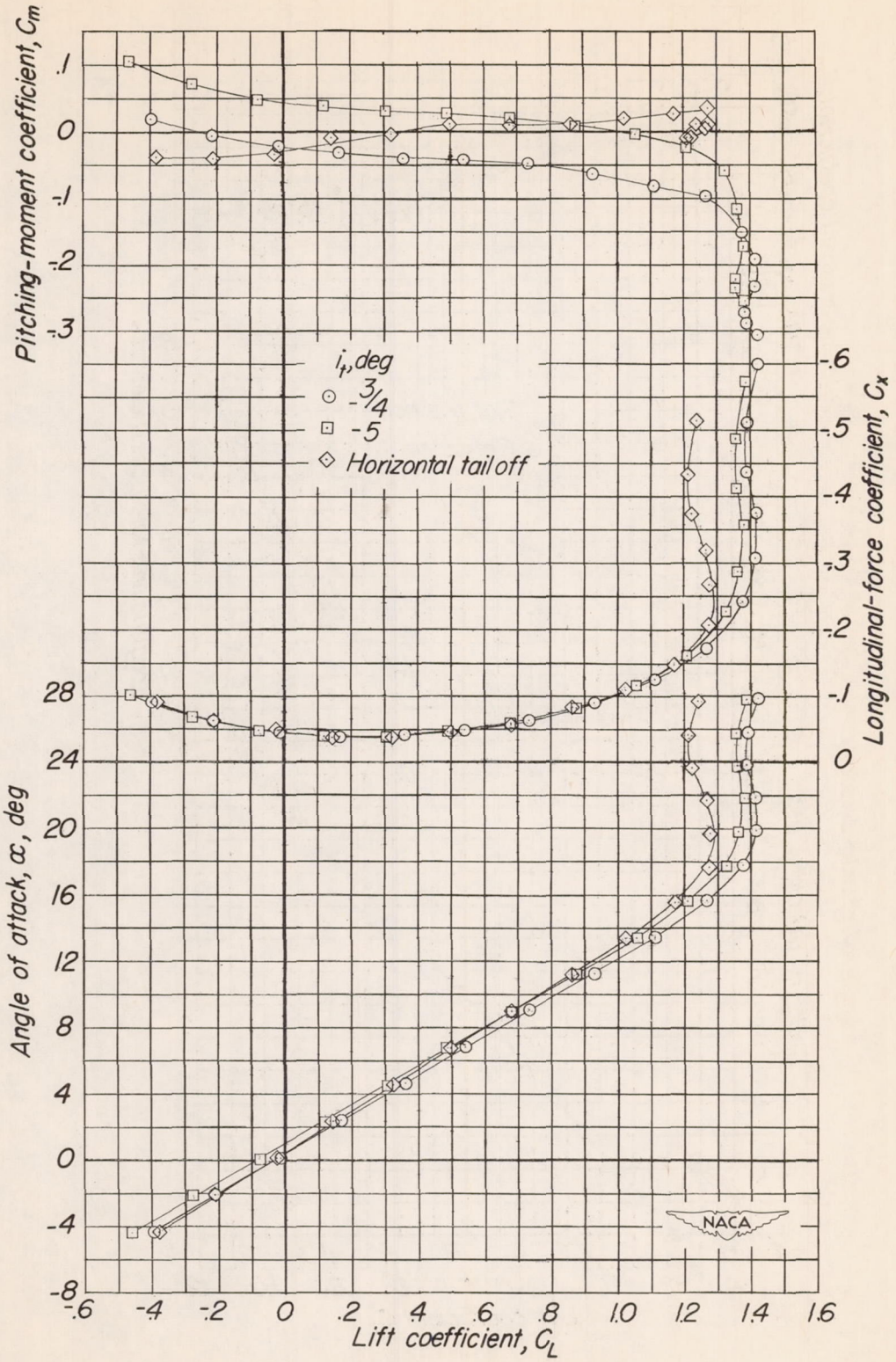

Figure 11.- The effect of tail incidence on the aerodynamic characteristics of the test model. $\Lambda = 20^{\circ}$, slat position A; $\delta_f = 0$.

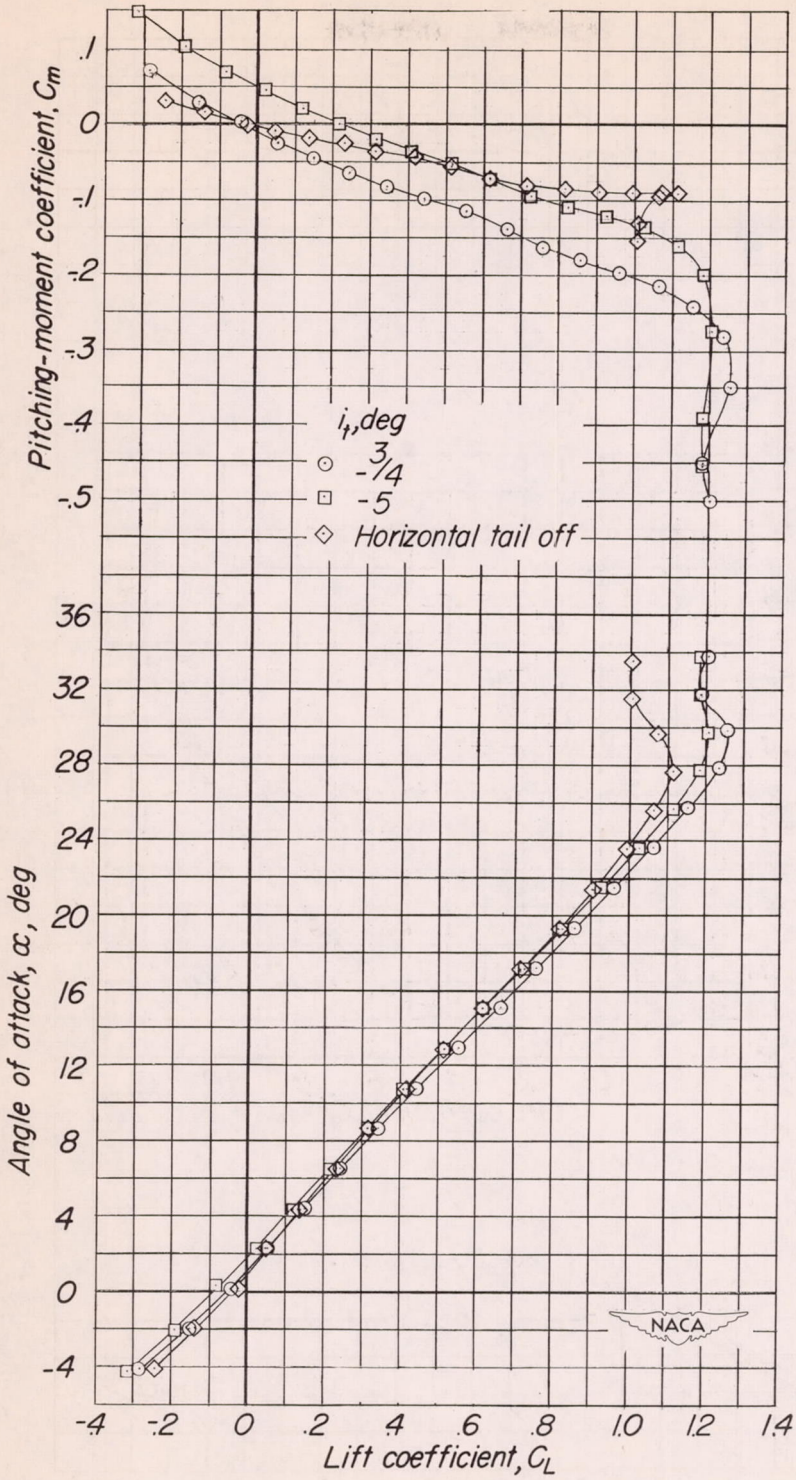

(a) Slat position A.

Figure 12.- The effect of tail incidence on the aerodynamic characteristics of the test model. $\Lambda = 60^\circ$; $\delta_f = 0$.

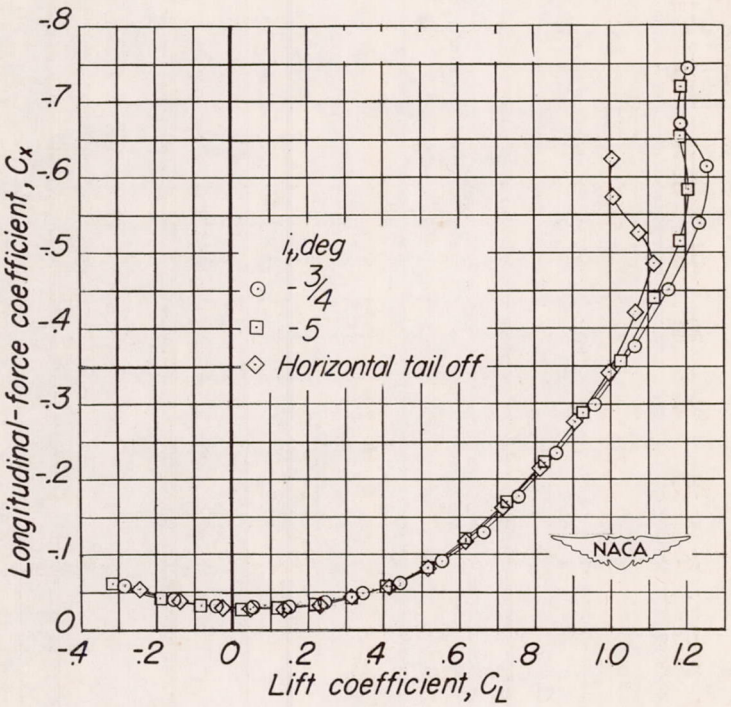

(a) Concluded.

Figure 12.- Continued.

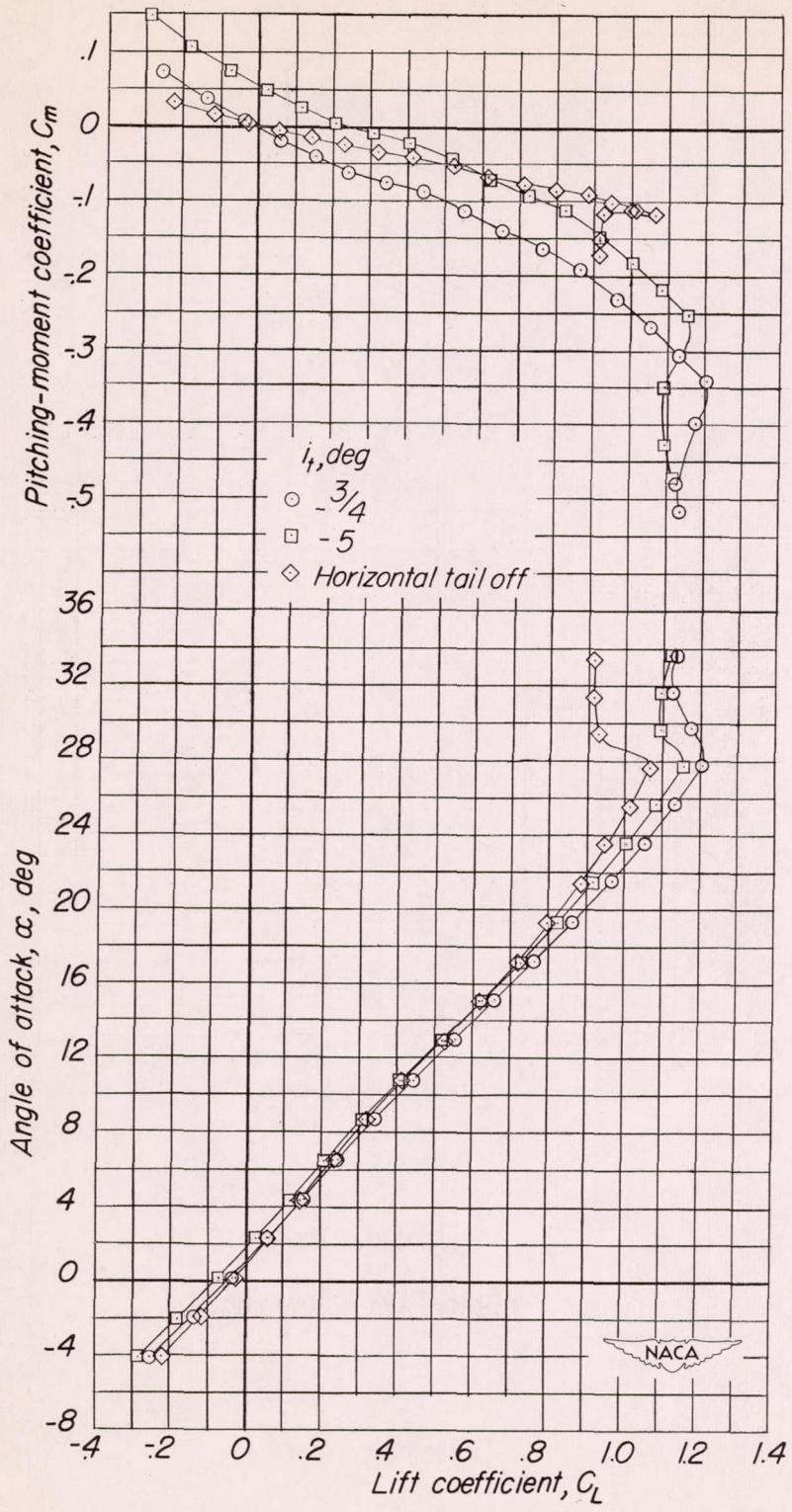

(b) Outboard half of slat at position A.

Figure 12.- Continued.

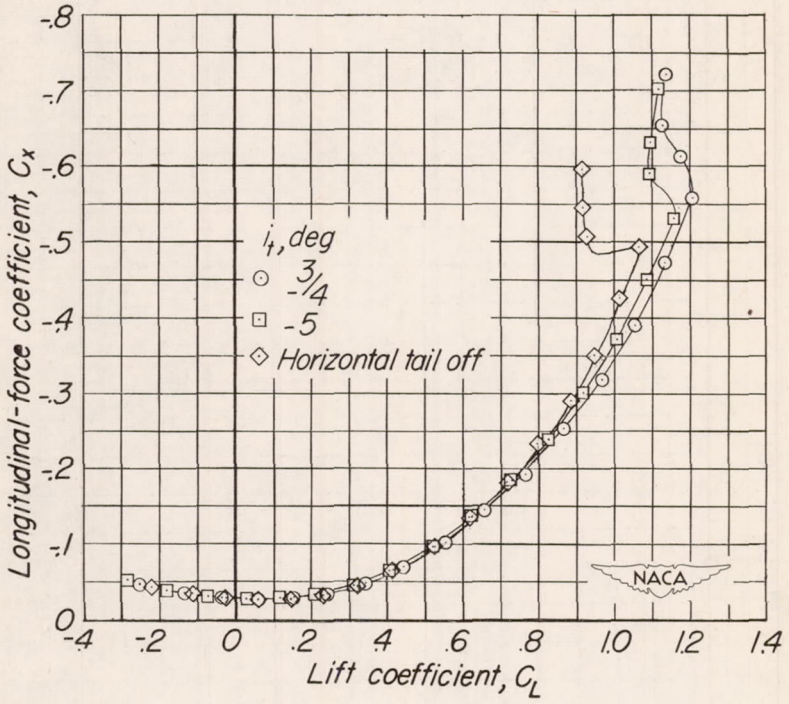

(b) Concluded.

Figure 12.- Concluded.

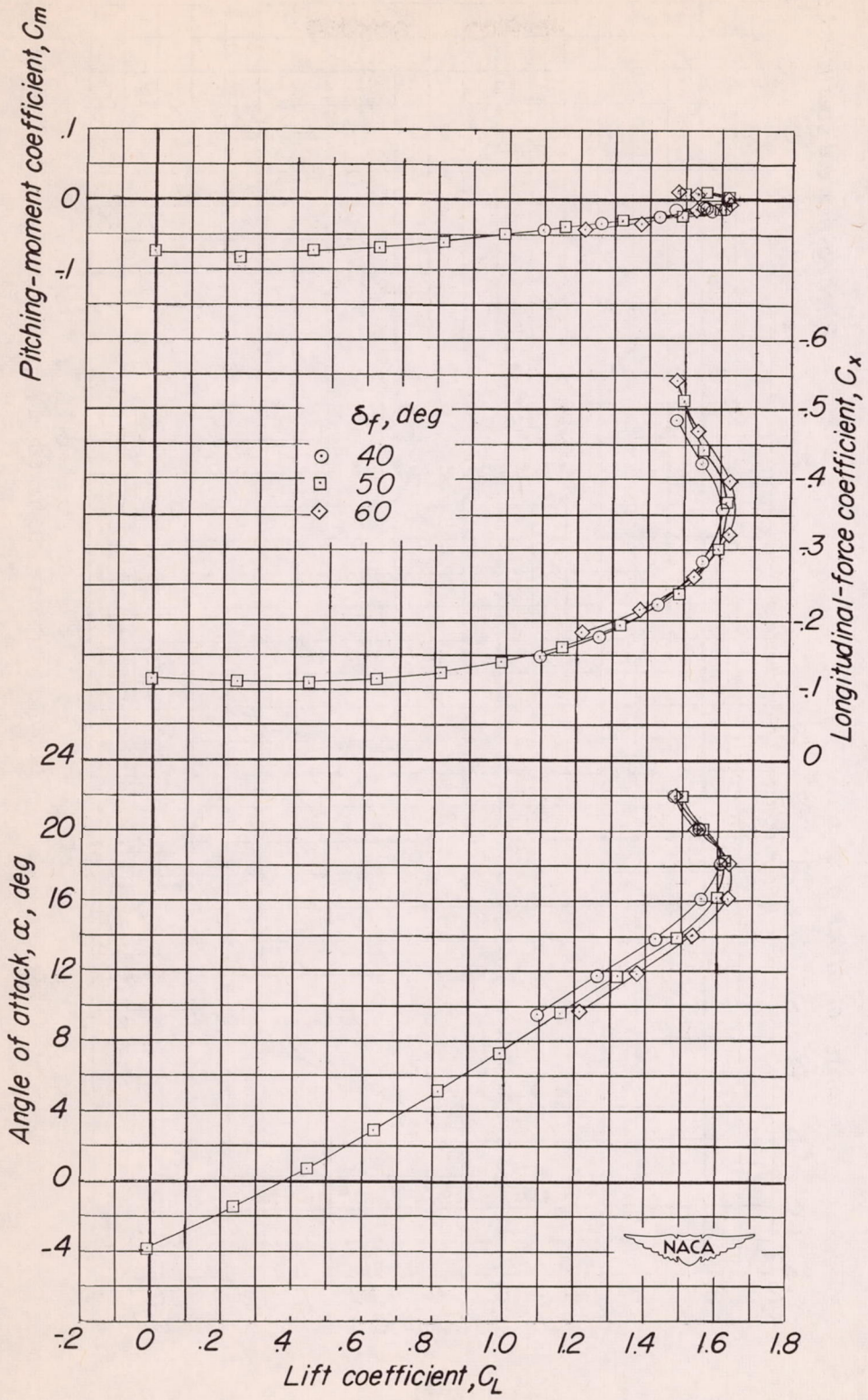

Figure 13.- The effect of flap deflection on the aerodynamic characteristics of the test model. $\Lambda = 20^{\circ}$; slat position A; horizontal tail off; flap B.

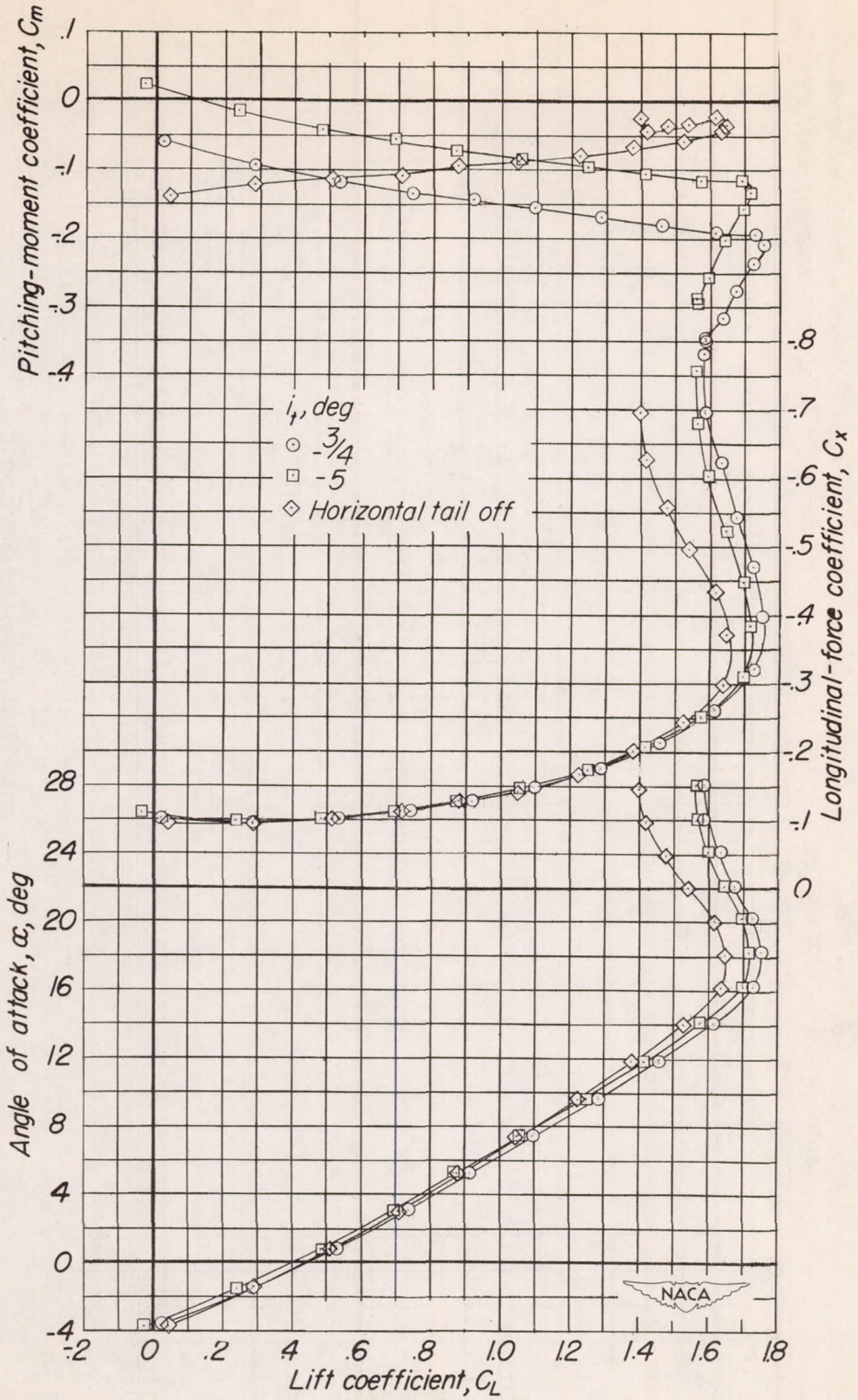

(a) Flap A.

Figure 14.- The effect of tail incidence on the aerodynamic characteristics of the test model. $\Lambda = 20^{\circ}$; slat position A; $\delta_f = 50^{\circ}$.

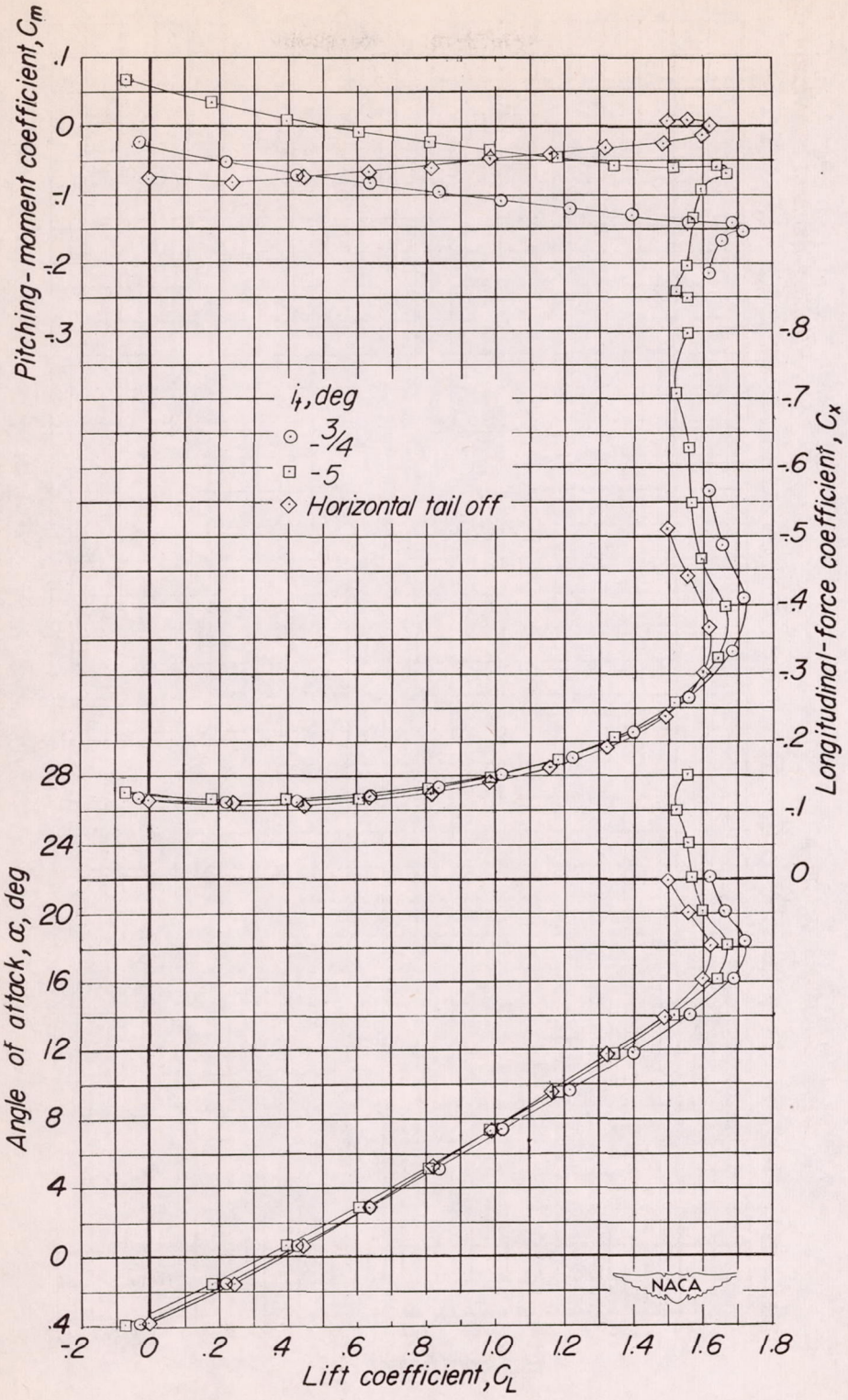

(b) Flap B.

Figure 14.- Continued.

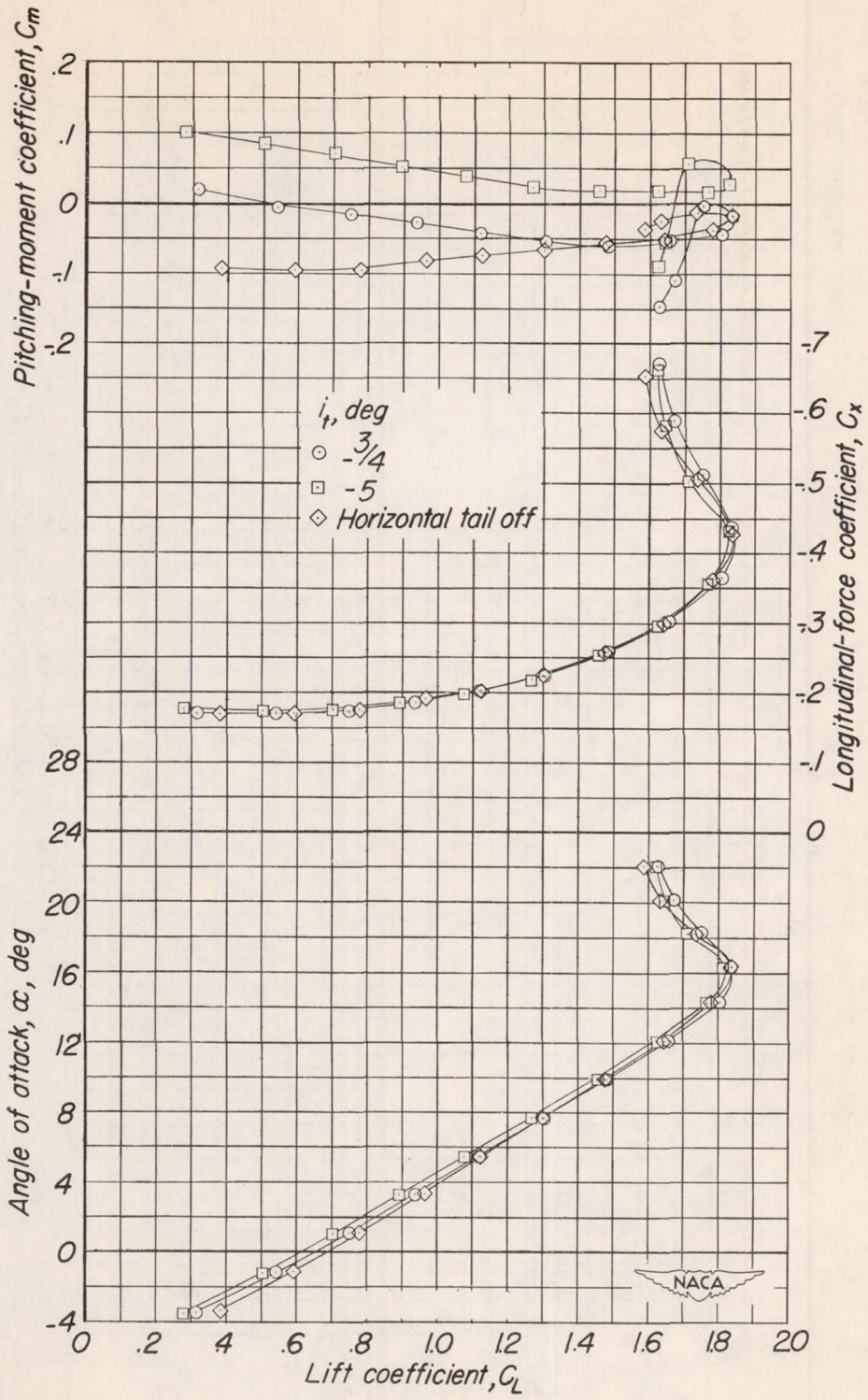

(c) Flap C.

Figure 14.- Concluded.

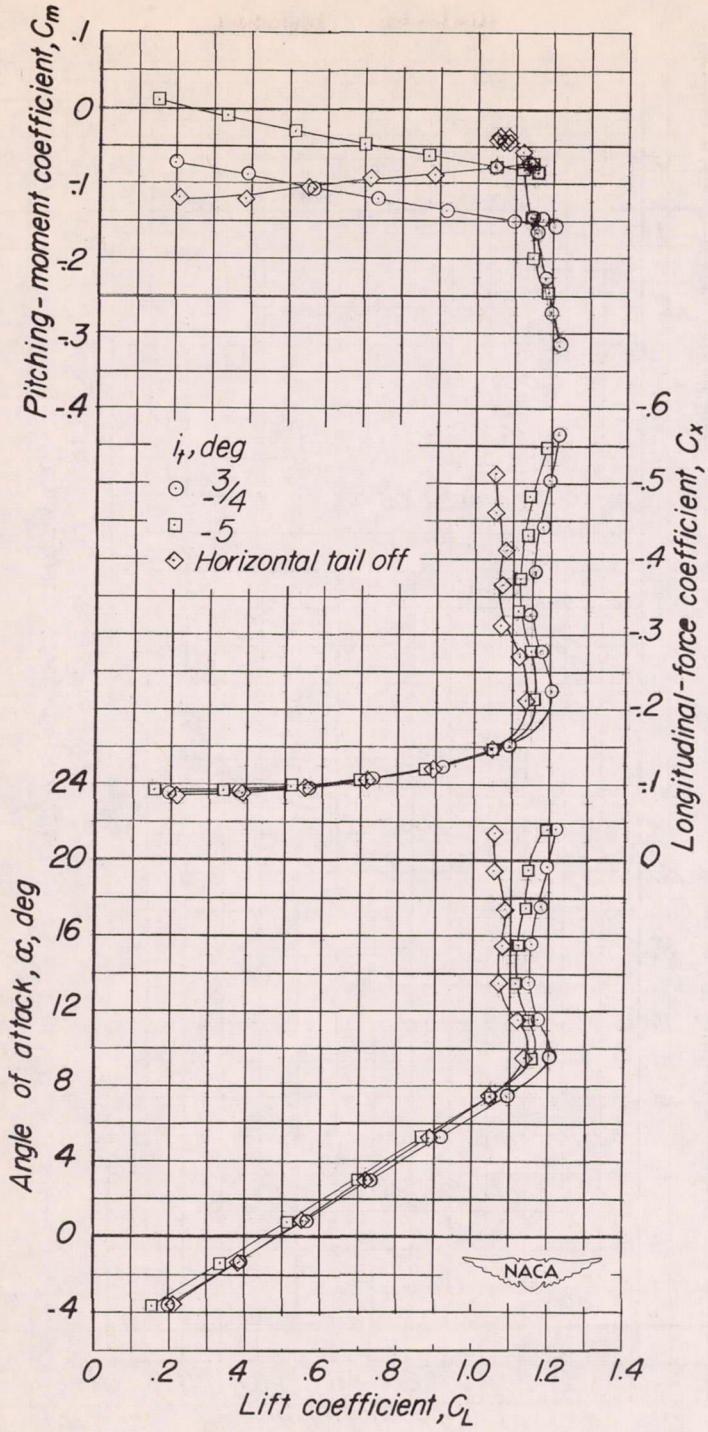

(a) Flap A.

Figure 15.- The effect of tail incidence on the aerodynamic characteristics of the test model. $\Lambda = 20^\circ$; slats retracted; $\delta_f = 50^\circ$.

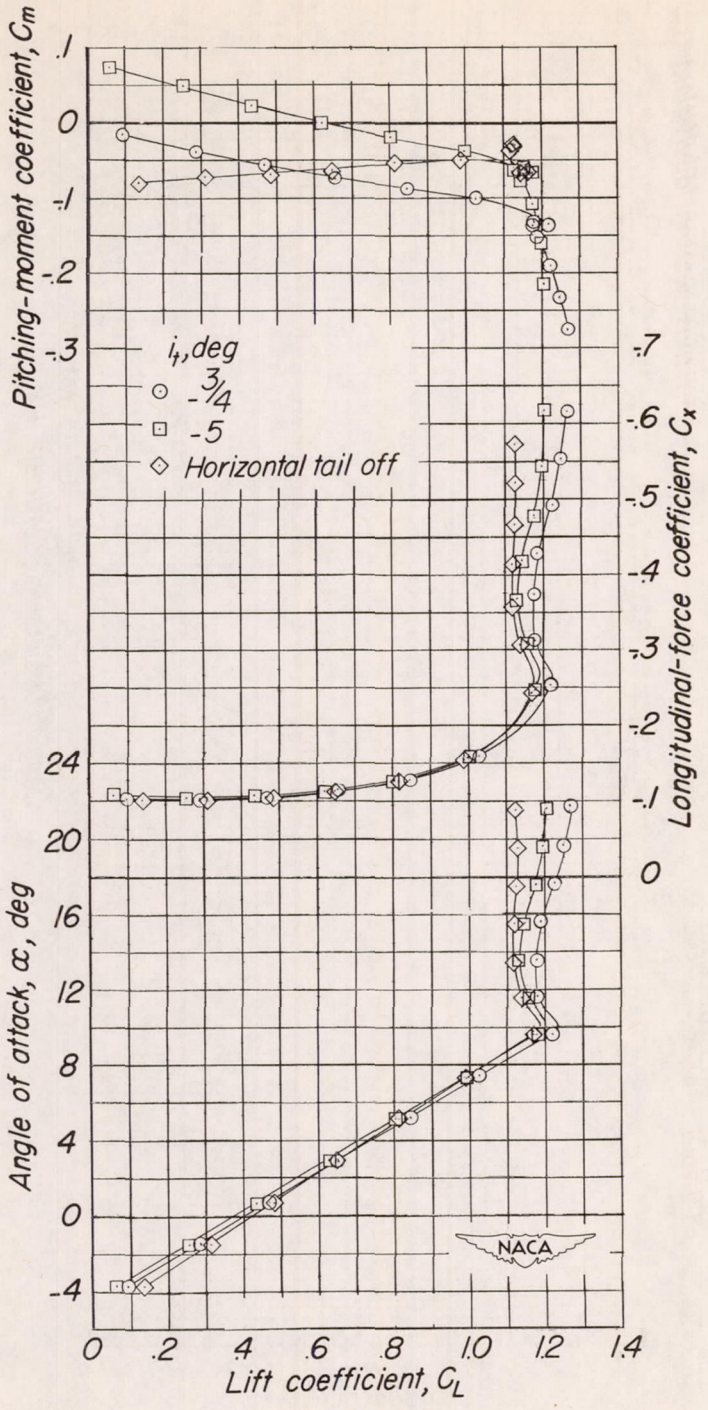

(b) Flap B.

Figure 15.- Continued.

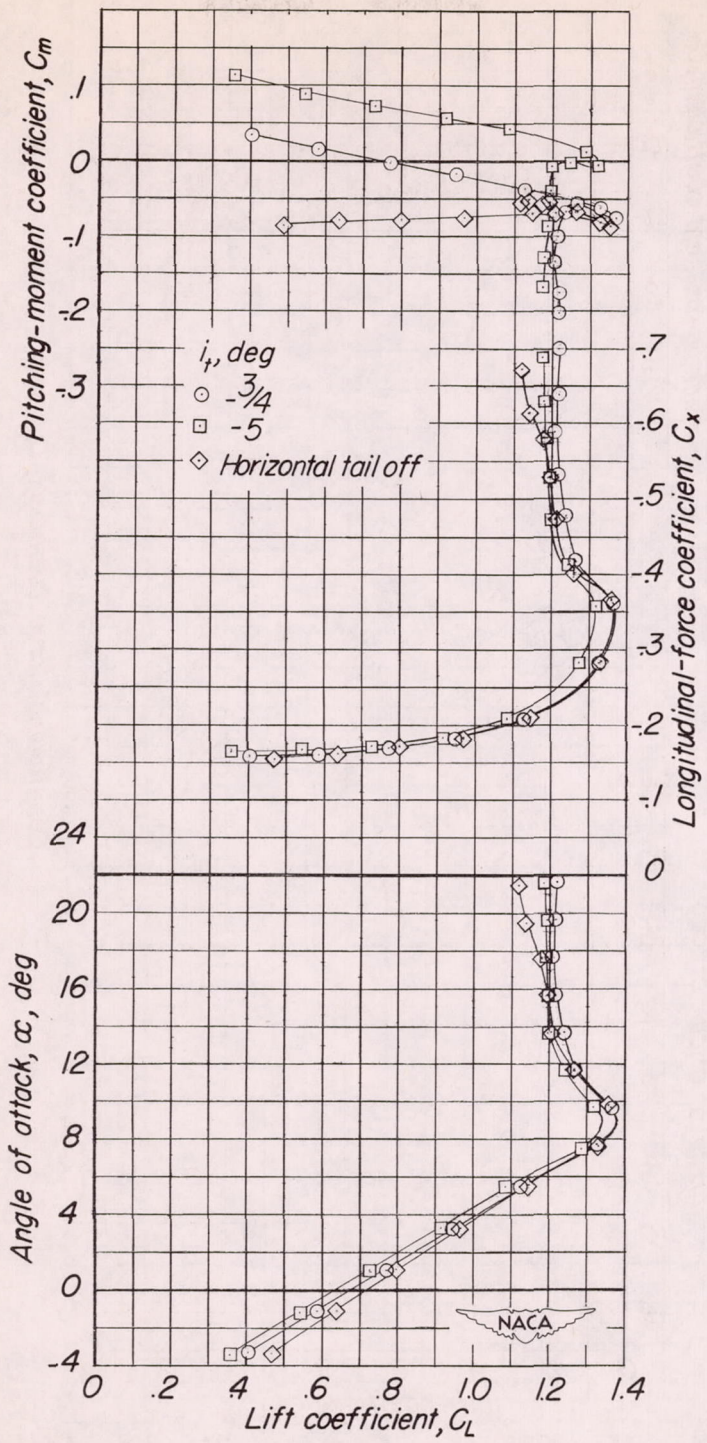

(c) Flap C.

Figure 15.- Concluded.

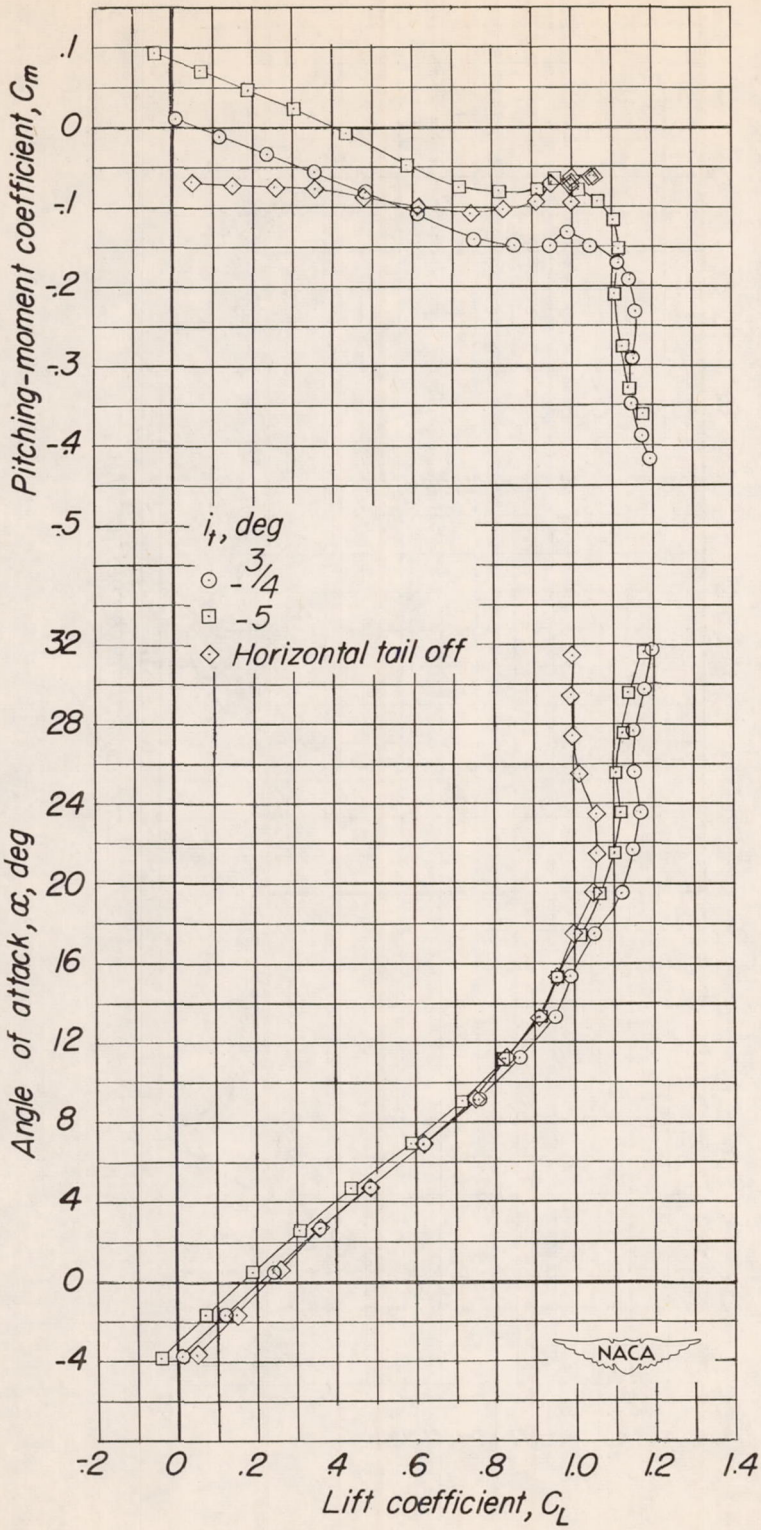

Figure 16.- The effect of tail incidence on the aerodynamic characteristics of the test model. $\Lambda = 50^\circ$; slats retracted; flap B; $\delta_f = 50^\circ$.

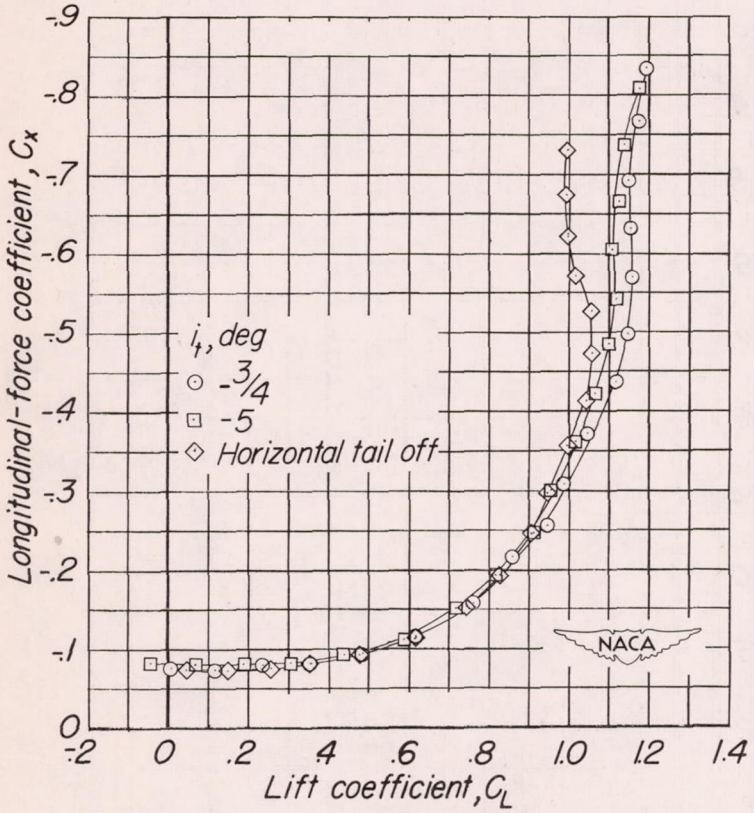

Figure 16.- Concluded.

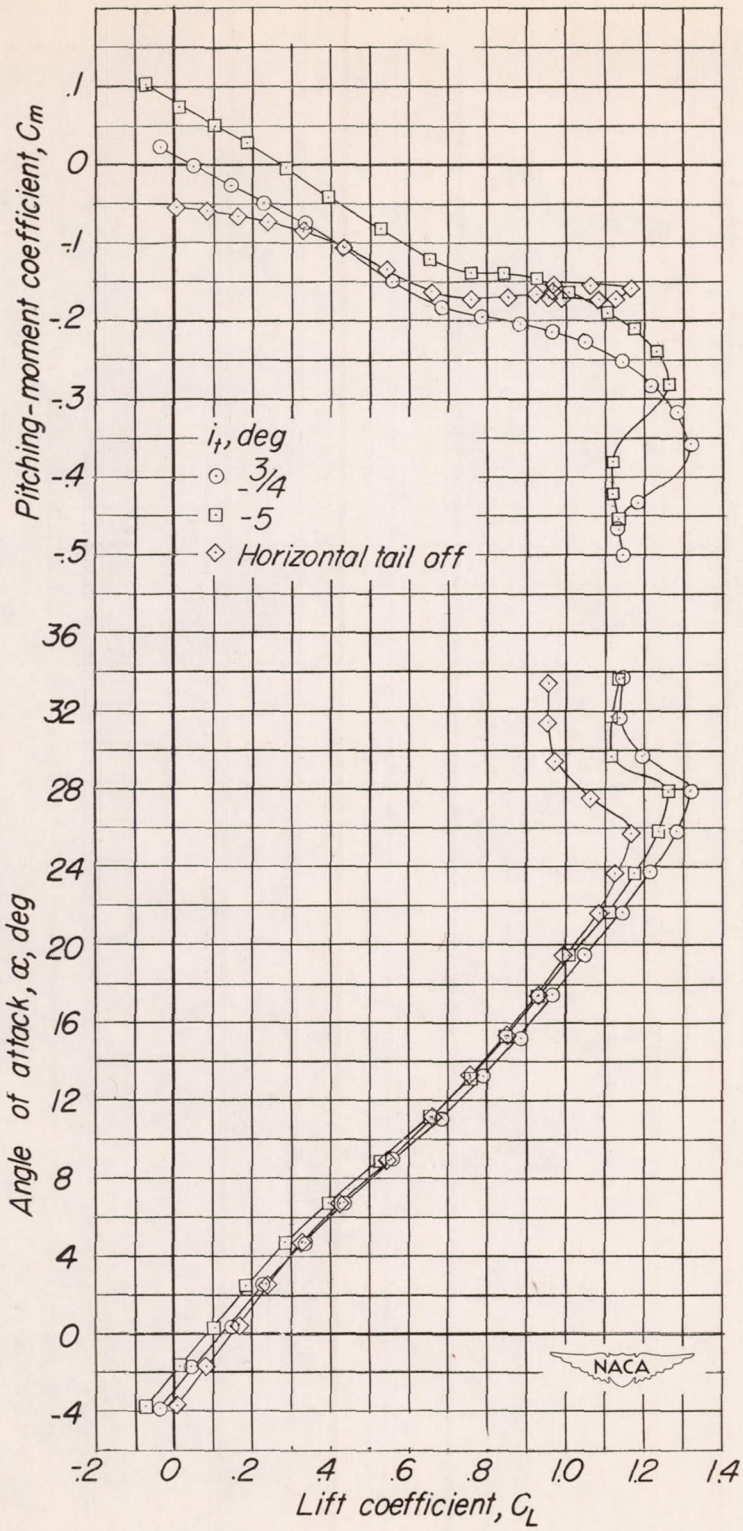

Figure 17.- The effect of tail incidence on the aerodynamic characteristics of the test model. $\Lambda = 60^\circ$; slats retracted; flap B; $\delta_f = 50^\circ$.

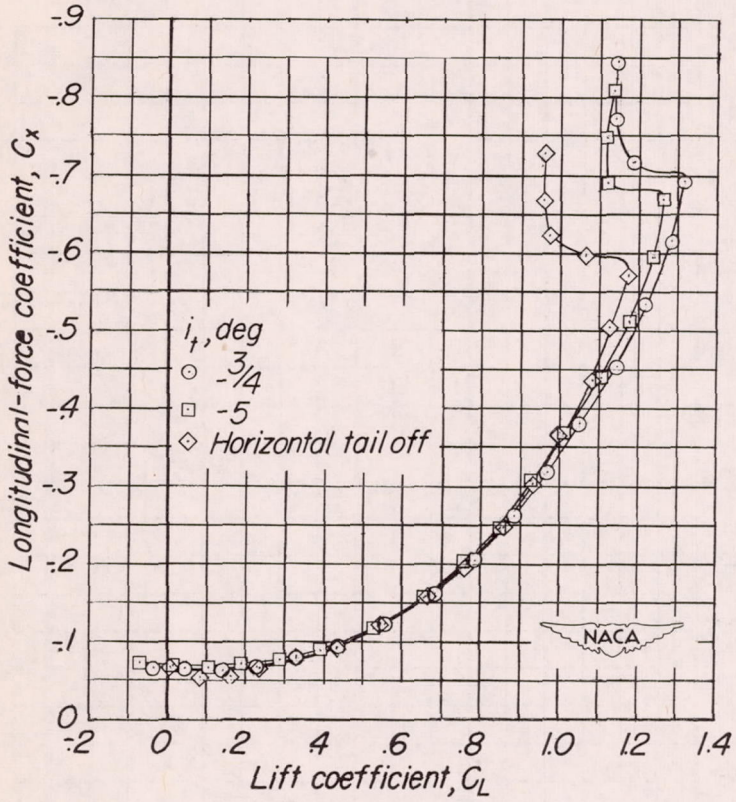

Figure 17.- Concluded.

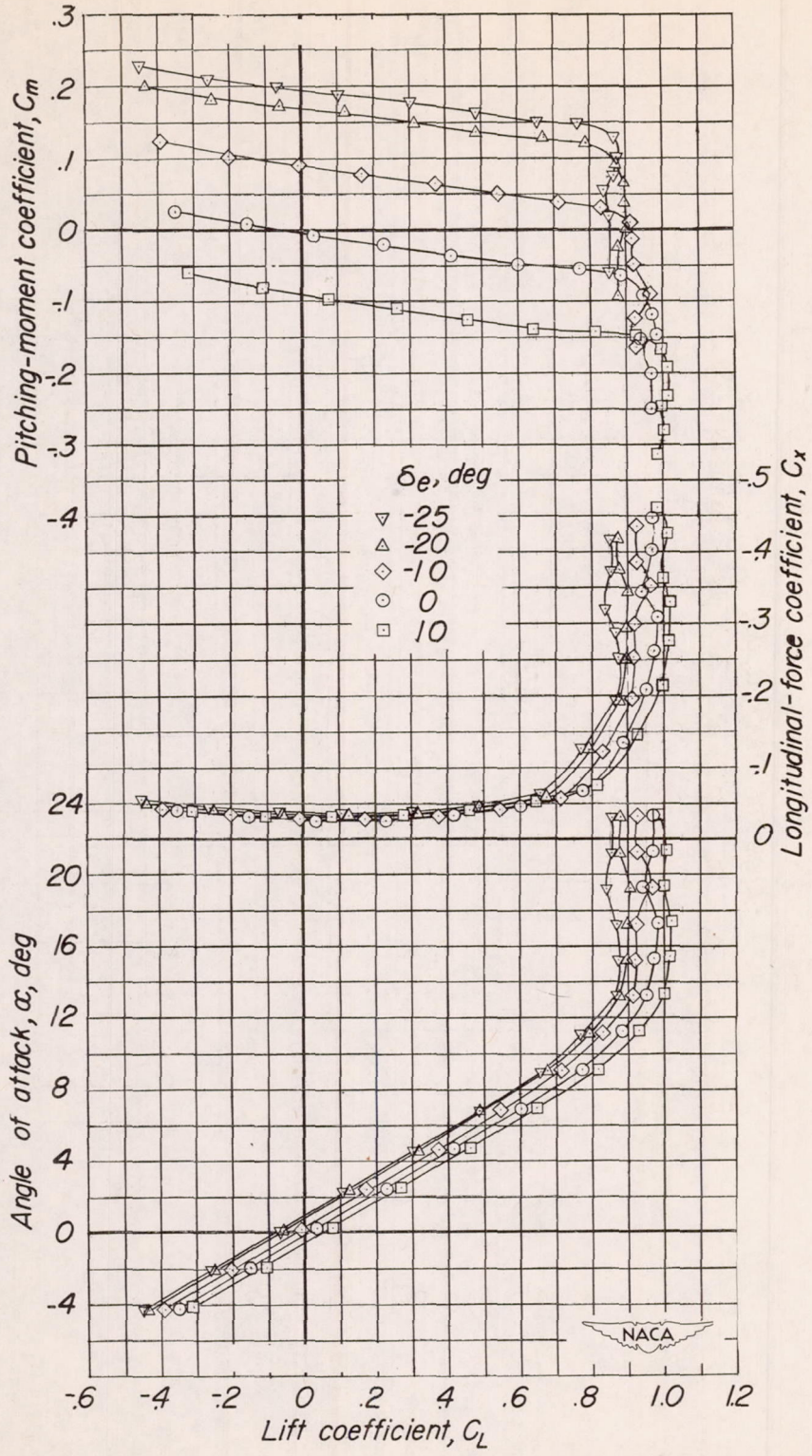

(a) $\Lambda = 20^\circ$; $i_t = -\frac{3}{4}^\circ$.

Figure 18.- The effect of elevator deflection on the aerodynamic characteristics of the test model. Slats retracted; $\delta_f = 0$.

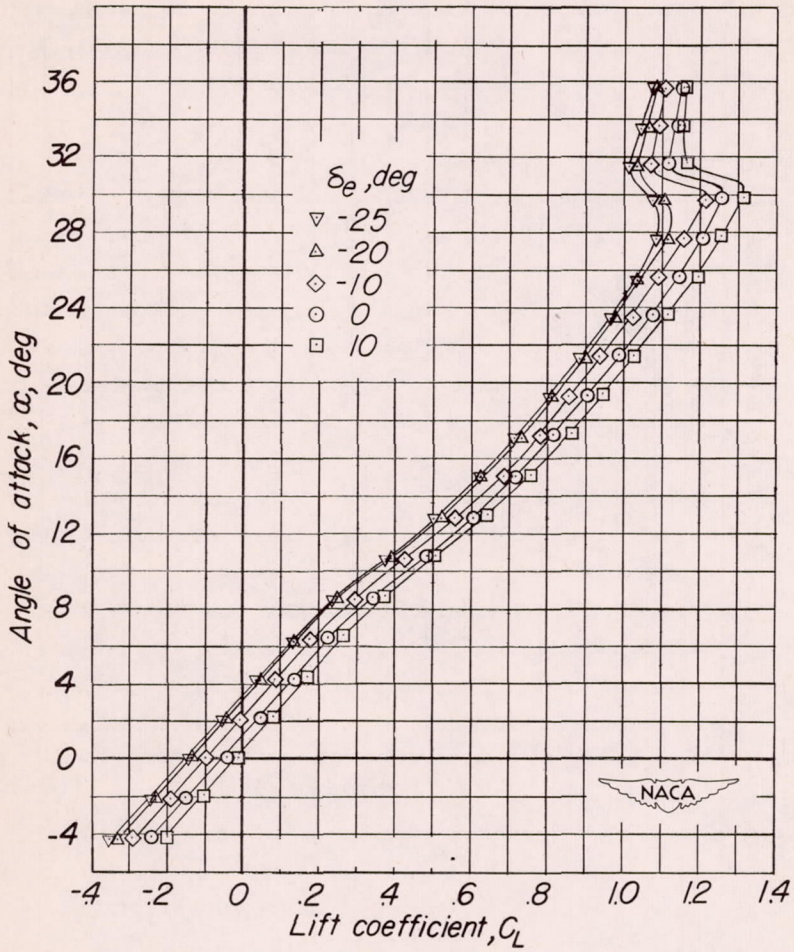

(b) $\Lambda = 60^\circ$; $i_t = -5^\circ$.

Figure 18.- Continued.

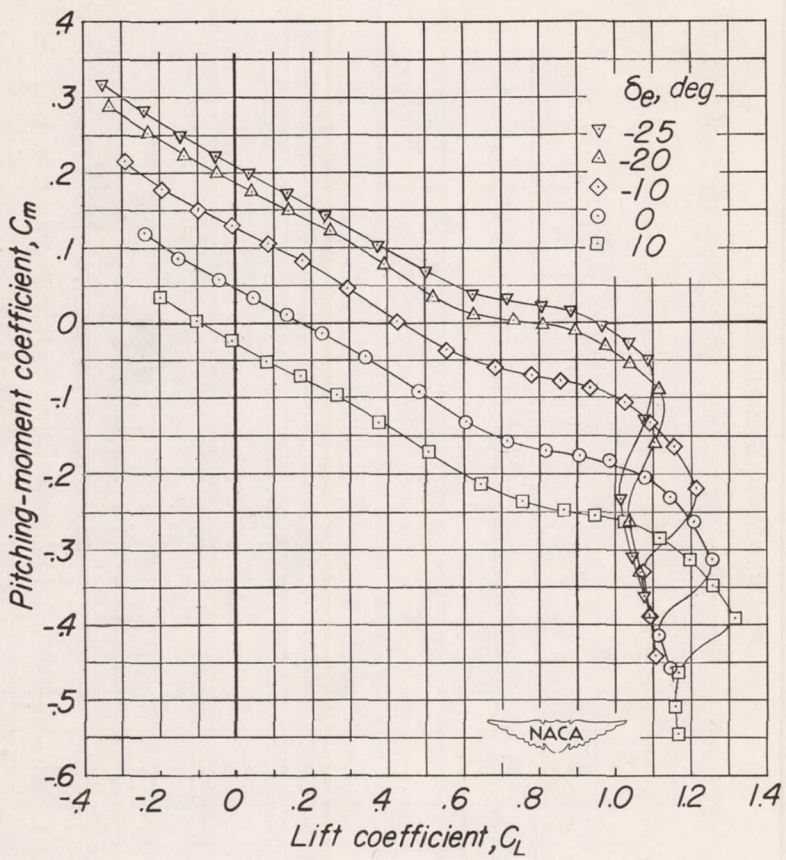

(b) Continued.

Figure 18.- Continued.

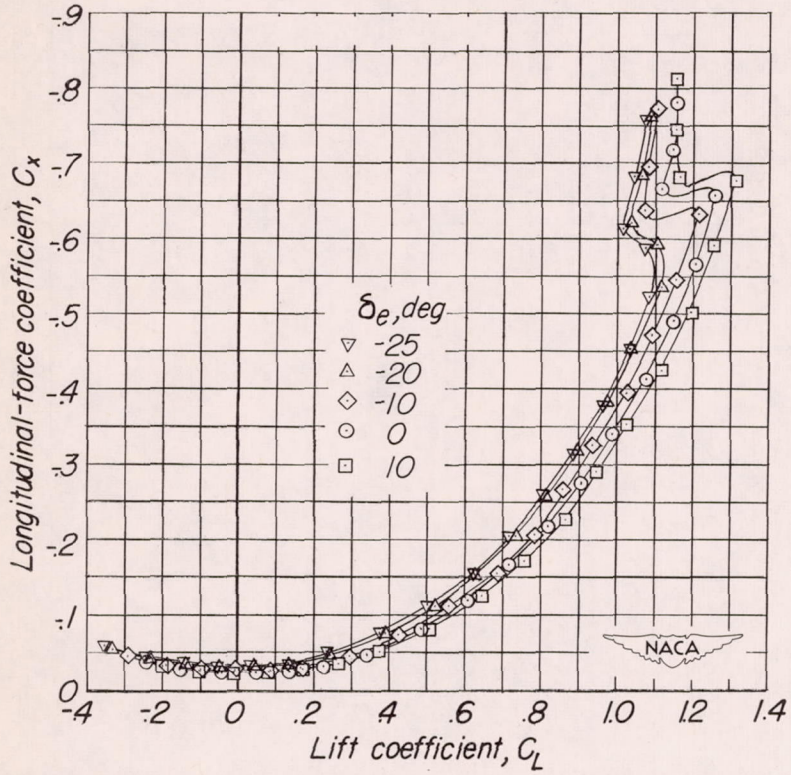

(b) Concluded.

Figure 18.- Concluded.